Ecological Indicators 178 (2025) 113869

Contents lists available at ScienceDirect

Ecological Indicators

journal homepage: www.elsevier.com/locate/ecolind

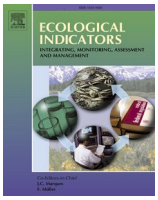

Assessing early bark beetle infestation in Norway spruce using multitemporal hyperspectral UAV imagery: Is detection during the green stage always timely?

Salma Bijou, Lucie Kupková *, Lucie Červená, Jakub Lysák

Department of Applied Geoinformatics and Cartography, Faculty of Science, Charles University, Albertov 6, Prague 2, Czech Republic

ARTICLE INFO

Keywords:
Bark beetle
Ips typographus
Norway spruce
UAV hyperspectral multitemporal imagery
Green stage
Timely detection
The Krkonoše Mountains

ABSTRACT

The European spruce bark beetle (*Ips typographus*) poses a major threat to forests, causing significant tree mortality and ecosystem disruption. Hyperspectral imagery from unmanned aerial vehicles (UAVs) offers potential for early detection of infestations, but its application remains limited. This study evaluates the effectiveness of a dense time series of UAV hyperspectral imagery (nine dates, May–August 2022, Krkonoše Mts. Czechia, 1030 m a.s.l.) at 3 cm spatial resolution for timely detection of bark beetle infestations in Norway spruce (*Picea abies (L.) Karst.*). We compared 23 infested trees (grouped into 11, 6, and 6) with 23 healthy controls (same grouping). Spectral separability between healthy and infested trees was assessed using Jeffries-Matusita distance, Analysis of Similarities, Wilcoxon rank-sum test, and Difference-in-Differences. The earliest detection date was June 15, ~3 weeks after estimated start of infestation, ~2 weeks after bark symptoms became visible, and ~2 weeks before crown discoloration appeared. To improve the timing and targeting of RS-based detection, we proposed subdividing the green stage into three substages: G-HS (green hidden symptoms stage, ca 1–10 days after start of infestation): subtle bark symptoms hidden in upper trunk, G-BS (visible bark symptom stage, lasts ca 3 weeks): visible bark symptoms in lower trunk, green crowns, G-YS (green-yellow stage, ca 5 weeks after bark visible infestation): initial crown discoloration. Our findings showed that UAV-based hyperspectral sensing can significantly enhance bark beetle detection, especially when the detection occurs within 3 weeks after bark-visible infestation providing a critical window for timely interventions to limit outbreak spread.

1. Introduction

Forests worldwide are undergoing substantial impacts due to climate change (Anderegg et al., 2020; Allen et al., 2010; Lindner et al., 2010). Rising temperatures and altered precipitation patterns are intensifying droughts, wildfires, and outbreaks of pests and pathogens. Synergy of these factors is accelerating the global decline and degradation of forests (Přävälie, 2018; Kupková et al., 2018). In Europe, nearly one-third of forests are currently in decline (Maes et al., 2023). This situation has become a major concern for public authorities, who are focused on preventing further deterioration, as forests provide essential ecosystem services such as water cycle regulation, biodiversity support, soil protection, and air quality improvement Hlásny et al., 2021). They also play a crucial role in carbon sequestration and storage, which is vital for mitigating the impacts of climate change (Nahuz et al., 1990; Pretzsch et al., 2023).

One of the most pressing sustainability challenges for forests is their high vulnerability to insect outbreaks (Sikorski et al., 2023; Forzieri et al., 2021). While such outbreaks are a natural component of forest dynamics, they become alarming when severe infestations shift from endemic to epidemic stages, causing significant tree mortality (Housecroft, 2023). The extreme drought in Central Europe in 2018 triggered some of the most severe insect outbreaks in history (Knutzen et al., 2023; Pirtskhalava-Karpova et al., 2024). The European spruce bark beetle (*Ips typographus*) has been the primary insect responsible for widespread damage to Norway spruce (*Picea abies (L.) Karst.*) forests (Stříbrská et al., 2023). Central European countries such as Czechia, Germany, Slovakia, Poland and Austria are the most severely affected both economically and ecologically by the bark beetle (Hlásny et al., 2021; Murray, 2006; Lausch et al., 2013). In 2022, Czechia reported the

* Corresponding author.
E-mail addresses: bijous@natur.cuni.cz (S. Bijou), lucie.kupkova@natur.cuni.cz (L. Kupková), lucie.cervena@natur.cuni.cz (L. Červená), lysak@natur.cuni.cz (J. Lysák).

https://doi.org/10.1016/j.ecolind.2025.113869
Received 2 February 2025; Received in revised form 17 June 2025; Accepted 7 July 2025
Available online 10 July 2025

extraction of over 5.6 million cubic meters of spruce wood infested by the bark beetle (Lubojacký et al., 2023).

Bark beetles are living under the bark, and typically favour trees over 60 years old with a diameter at breast height exceeding 20–25 cm (Zimová et al., 2020; Müller et al., 2022). They usually begin swarming when daytime temperatures reach approximately 16.5 °C (Doležal and Sehnal, 2007; Lausch et al., 2013). The beetles can survive through winter and complete several generations annually (Brázdil et al., 2022; Hlásny et al., 2021).

Bark beetle infestation in spruce trees progresses through several lifecycle stages. Initially, shortly after swarming and a successful attack, male beetles bore into the tree and release pheromones to attract females. This stage, known as initial colonization, involves the creation of mating chambers and maternal galleries where eggs are laid. As at the beginning of infestation the adults bore into the upper parts of the trunk (Lubojacký et al., 2018; Kautz et al., 2024), and frass and resin ducts are minimal at this stage, especially if the attack is not widespread, the symptoms are hidden and hard to detect. Consequently, no visible symptoms are typically present on the lower parts of the trunk at this stage. According to our experience and some studies (Wermelinger and Seifert, 1998; Kautz et al., 2024; Bárta et al., 2022; Berec et al., 2013; Webb et al., 2024, Lubojacký et al., 2018, Kautz et al., 2023), this period of "hidden" symptoms can range approximately few days up to 2 weeks, depending on environmental factors such as temperature, humidity, tree resistance. Given a sufficiently high beetle population density, subsequent attacks continue downwards, resulting in a full coverage of the stem with galleries.

The symptoms such as boring holes, resin flow and boring dust become visible in the lower parts of the trees. Finally, as the infestation progresses, the tree's health deteriorates further, leading to crown discoloration (yellowing, and later reddening of needles), which generally becomes visible around approx. 4–8 weeks after the initial attack (Bozzini et al.; 2024; Huo et al.; 2023a, Bijou et al.; 2023, Lubojacký et al., 2018).

The spread of infestation can rapidly cover large areas, and existing traditional field methods of detection (field surveys and visual inspections) are both time-consuming and labor-intensive. Identifying infested trees promptly for removal in the field using traditional methods poses a real challenge, as they require frequent visits across extensive areas. Remote sensing (RS) has proven to be an efficient tool in spotting foliar discoloration from successful bark beetle attacks (Abdullah et al. 2018), ideally directing ground surveys to identify trees with possible symptoms of infestation (Nardi et al. 2023).

Multitemporal imagery with high spatial and spectral resolution, particularly hyperspectral data from UAVs or aerial imagery, offer the greatest potential for early detection. Although spatially detailed imagery has become more common for GS detection, hyperspectral data have been used only to a limited extent. Huo et al. (2023a) used UAV multispectral imagery with 6 cm resolution and detected 15 % of GS-infected trees after 5 weeks, improving to 87 % at 10 weeks when crown discoloration was visible. Klouček et al. (2024) evaluated GS infestation with UAV multispectral data from July 29, identifying differences between healthy and infested trees using NIR-based VIs like NDVI and BNDVI. Bozzini et al. (2024) detected infestation one month before visible symptoms appeared using UAV multispectral imagery and indices such as NDVI, SAVI, and NDRE. Bárta et al. (2022) analyzed airborne hyperspectral imagery with 48 bands at 0.5 m resolution, detecting reflectance changes after 23 days of infestation. The most successful VIs included REIP, PRI, and ANCB650–720 within 6 weeks. In contrast, Huo et al. (2024) found low detection rates using UAV hyperspectral imagery at 10 cm GSD, with 0.3 % detectability after 5–7 weeks and 0.8 % at 7–9 weeks.

RS methods for detecting bark beetle infestation include vegetation indices (VIs), spectral band analysis, statistical techniques, and supervised classifications. Key spectral bands like the red-edge (Hellwig et al., 2021) and shortwave infrared (Huo et al., 2021; Abdullah et al., 2018) are effective for distinguishing healthy from infested trees. The red band is also frequently used (Huo et al., 2021; Bijou et al., 2023). NIR (Near-Infrared) bands are less effective for early detection (Bijou et al., 2023; Klouček et al., 2019), except in lab studies (Abdullah et al., 2018). Sentinel-2 with red-edge and water-related indices outperformed Landsat 8 for identifying green stage trees in the study of Abdullah et al. (2018). NIR-based indices such as NDVI (Klouček et al., 2024) and EVI/VARI (Trubin et al., 2024) also showed good results. Novel indices like the Multiple Ratio Disease–Water Stress (Huo et al., 2023a) and the NDRS (Huo et al., 2021) have been proposed, with the latter achieving 80–82 % accuracy. Bárta et al. (2021) reported 78 % accuracy using TCW and NIR–SWIR, and Näsi et al. (2015) achieved 90 % accuracy for two-class classification with hyperspectral sensors, dropping to 76 % with a third class (infested).

From a management perspective, it is critical to start monitoring the infestation symptoms as soon as possible after a suspected attack, as this time is crucial for an early/timely detection and sanitary logging. Using the symptoms of the foliage/crown discoloration, the bark beetle infestation is classified into four distinct stages. Initially, spruce trees show no visible symptoms of infestation on foliage (Green stage – GS), followed by yellowing of leaves (Yellow stage – YS), indicating severe stress. In the Red stage (RS), trees show red leaves, signifying irreparable damage and a peak in bark beetle populations. Eventually, in the Grey stage (GRS), trees die, and their leaves turn grey and fall off (Niemann and Visintini, 2005).

Studies across various sensors and regions showed that the earliest foliar color changes of infestation (for overwintered generation) occur in July or August, depending on the study area, meaning the GS typically lasts from May to July, i.e., 4–8 weeks or more (Bozzini et al., 2024; Huo et al., 2023a). The new filial generation can emerge 6 to 10 weeks after infestation, depending on temperature and precipitation, with trees potentially still appearing green (Webb et al., 2024; Bárta et al., 2022; Kautz et al., 2023). Early detection is crucial for forest management, ideally before the new generation emerges, as sanitation measures must be implemented before beetles spread further. Detection during the late GS (shortly after initial crown discoloration and before new filial emergence) may already be ineffective. Therefore, defining substages within the GS based on phenology and field symptoms is important for identifying the critical window when RS can still enhance management. Few studies have addressed these substages. Kautz et al. (2024) outlined two substages but omitted the yellow stage, which misrepresents infestation progression. Dalponte et al. (2023) identified G1 and G2 substages but included needle and bark loss in G2, which typically occurs in later stages. While stage progression is continuous and influenced by many factors in the field, examining the GS in greater detail is still particularly relevant, especially in the context of RS effectiveness evaluation.

As evidenced in the above mentioned studies and also summarized by Kautz et al. (2024), some studies have detected the GS. However, they focus mainly on its later stage, missing the critical early window at infestation onset. Time series usually cover no more than five dates and rely on multispectral imagery across the full season, lacking the temporal density of early high-frequency hyperspectral data needed to capture initial spectral changes. Ground truth at the tree level and clear definitions of infestation stages are often missing. These gaps limit the RS applicability in detecting and preventing bark beetle outbreaks.

To address these gaps, our study employs a unique dense time series of UAV-based hyperspectral images with 3 cm spatial resolution, acquired on nine dates before and during infestation, combined with detailed ground truth for each date. We evaluate the effectiveness of these data for early detection of bark beetle infestation in Norway spruce (*Picea abies (L.) Karst.*) using Jeffries-Matusita distance, Analysis of Similarities, Wilcoxon rank-sum test, and Difference-in-Differences methods. As early detection is crucial for efficient bark beetle management and outbreak prevention, we focus on the following research questions:

1) How early within the green stage, and in which spectral region, can discernible differences between healthy and infested trees be first detected using dense time series of UAV-based hyperspectral imagery and the above-mentioned statistical methods?
2) What are the key milestones in the progression of a bark beetle infestation during the green stage that remote sensing should be able to detect in order to enhance bark beetle management?
3) Is the spectral detection during the green stage always timely, or can it already be too late in the advanced green stage when aiming to accelerate sanitation measures and prevent further spread of the infestation?

2. Materials and methods

2.1. Study area and field data collection

The research was carried out during the 2022 growing season in a forest stand prone to bark beetle infestation (particularly *Ips typographus*) within the Krkonoše National Park (KRNAP), Czech Republic. Historically associated with forestry and mining, KRNAP, established in 1963, is the oldest national park in the country and protects a range of unique mountainous ecosystems. Forests cover approximately 79 % of its area, dominated by Norway spruce (*Picea abies*), with additional species including mountain pine (6 %), European beech (5 %), and other broadleaved trees (10 %). The study site, covering an area of approximately 4 ha, is a Norway spruce monoculture located near Dolní Dvůr (Tetřeví boudy chalet) in the Hradec Králové Region at an elevation of 1030 m a.s.L. (Fig. 1). The site is managed by the forestry service of the national park, and bark beetle infestations have been present there for several last years.

Monitoring of the study site began on 16 May 2022 and continued until 25 August. Field inspections were carried out in cooperation with trained KRNAP foresters, who regularly visited the plot and systematically assessed the bark, branches, and overall tree health to detect symptoms of bark beetle activity. At the start of the monitoring period (16 May), no infestation symptoms were observed and no trees showed signs of bark beetle attack. According to records provided by the foresters, the first visible symptoms, specifically boring holes and resin flow on the lower parts of the tree trunks, were detected on 3 June. The infestation then progressed in additional waves, likely triggered by parental beetles from the initial swarming event, over the following weeks (see Fig. 2). During the entire monitoring period, a total of 36 trees were infested. However, only 23 of these trees exhibited a clear progression of infestation (boring dust, color changes of foliage, defoliation, bark loss) within the observation period and were therefore retained for further analysis. Among them, infestation symptoms on the bark were first recorded on 3 June in 11 trees (Group G1), 12 days later on 15 June in 6 trees (Group G2), and 21 days later on 24 June in another 6 trees (Group G3). A detailed description of infestation progression of each group is described in chapter 3.1.

Infested trees were labelled in the field with a unique numerical identifier, and their exact positions were measured using a Trimble C5 total station to enable precise mapping in UAV-derived orthomosaics. The change in health status of each tree was evaluated based on visible infestation symptoms (including bark symptoms, crown discoloration, defoliation, and bark loss) throughout the entire monitoring period on each UAV data acquisition date (altogether 9 dates – for specific dates, see Fig. 2 and chapter 2.2.).

To serve as a control in the analysis, 23 healthy trees were selected and grouped into 11, 6, and 6 trees, respectively, to match the group

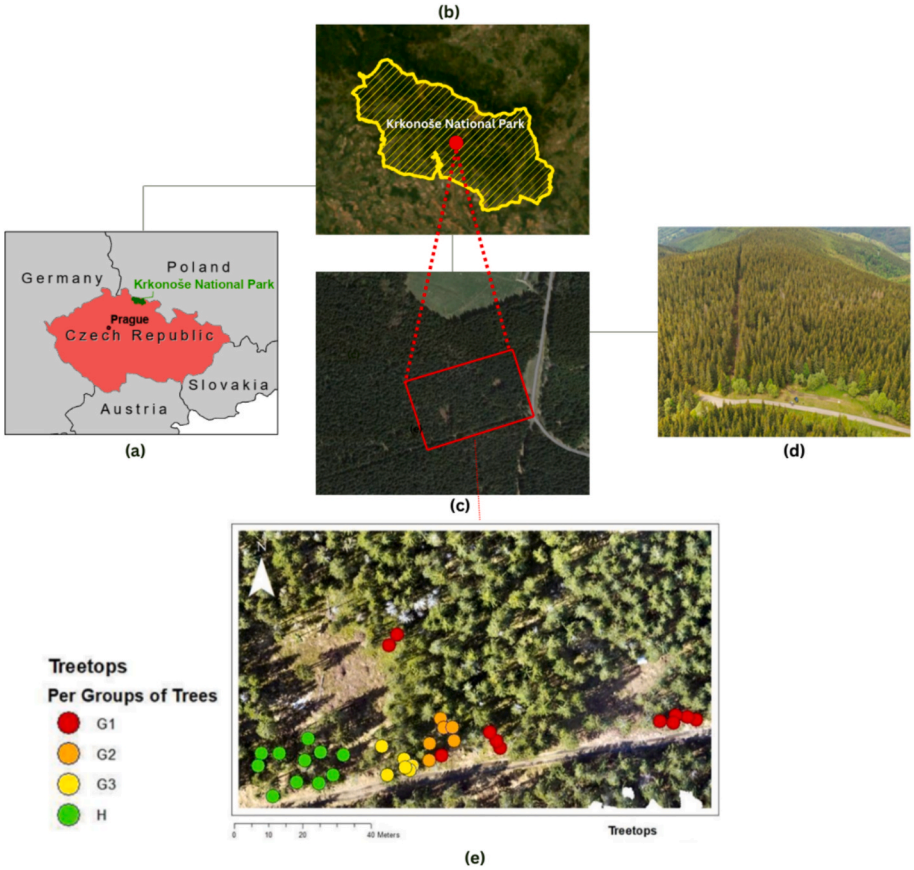

Fig. 1. Study area, including (a) Location of the Krkonoše National Park in the Czech Republic, and (b) the area of the Krkonoše National park, (c) Location of the forested plot where we conducted the research (Latitude = 50°39′57.4″N, Longitude = 15°41′36.6″E) (d) Drone picture of the forested area (e) Positions of the infested trees (G1, G2, G3) and healthy control trees used for the analysis (H: Healthy).

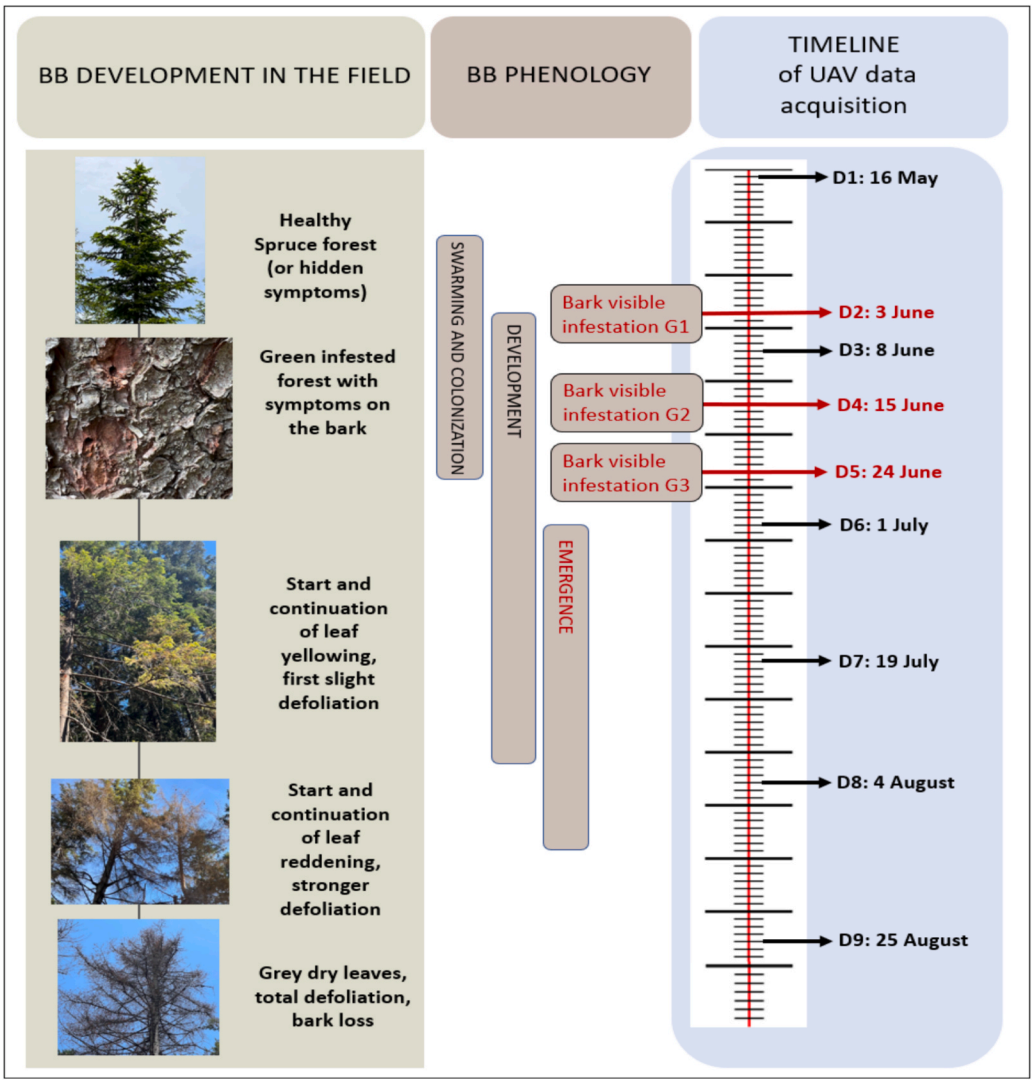

Fig. 2. Progression of bark beetle infestation in the field, combined with bark beetle phenology (of the overwintered generation), and a timeline showing the 9 dates of UAV data acquisition and the dates when the first visible bark symptoms (bark visible infestation) appeared in tree groups G1, G2, and G3 (highlighted in red). *Note: Bark beetle development and emergence were not modelled; the timing is only theoretical.* (For interpretation of the references to color in this figure legend, the reader is referred to the web version of this article.)

sizes of the infested trees and allow for direct comparison. The selection was based on two criteria: (1) maintaining a considerable distance from the plots of infested trees (approximately a 15-metre buffer), and (2) consistently healthy crown appearance throughout the observation period. Additionally, their health status was confirmed through NDVI thresholding prior to analysis. Only sufficiently illuminated pixels with NDVI values exceeding 0.7 were selected for the analysis. The locations of these selected healthy trees are shown in Fig. 1.

2.2. Estimation of the start of infestation using thermal sum data

Since visible bark symptoms do not appear immediately after infestation begins (Lubojacký et al., 2018, Kautz et al., 2023), we estimated the most likely start of bark beetle attack/infestation by calculating accumulated thermal sums, expressed in degree-days (DD). Temperature data were obtained from the Czech Hydrometeorological Institute (ČHMÚ, 2025), which maintains a long-term network of climatological stations with records dating back to 1961. We used data from the nearest station, located 5.5 km from the study site in Pec pod Sněžkou, to calculate daily thermal sums.

Two commonly used phenological models rely on temperature thresholds to estimate the start of infestation (Baier et al., 2007; Jönsson et al., 2007; Berec et al., 2013). These models differ in their input requirements, temperature metrics, and sensitivity to climatic variability. The Jönsson model accumulates degree-days above a base temperature of 5 °C using mean daily temperatures, starting from January 1. Swarming is estimated to occur when 120 cumulative degree-days (DD) are reached, but only if at least one day with a daily maximum temperature exceeding 16 °C is observed, reflecting the physiological threshold for flight activity. The PHENIPS model accumulates degree-days above a base temperature of 8.3 °C, using maximum daily temperatures starting on April 1, or on the first subsequent day when the maximum temperature exceeds this threshold. Swarming is assumed to begin when 60 cumulative DD are reached, but only if at least one day with a daily maximum temperature exceeding 16.5 °C.

A comparison of modeled cumulative degree-days based on the Jönsson and PHENIPS models for our study area is presented in Appendix A. The Jönsson model estimated the start of infestation on May 24, while the PHENIPS model on May 3. Due to the high diurnal temperature variation in our mountainous study area, we consider the Jönsson model more appropriate. Its input requirements are better aligned with the thermal regime of the site, making its prediction more

robust and ecologically plausible. Therefore, we consider the Jönsson model more appropriate for our study site, and May 24 as the most likely date of attack/infestation start.

2.3. UAV imagery collection

We gathered UAV data at nine time points between May 16 and August 25, 2022. The specific dates were May 16, June 3, June 8, June 15, June 24, July 1, July 19, August 4, and August 25 (Fig. 2). Two flights were conducted on each date. The first flight captured hyperspectral imagery (400–1000 nm, 269 bands) using a Headwall Nano-Hyperspec sensor mounted on a DJI Matrice 600 Pro. The second flight collected RGB and multispectral imagery (blue, green, red, red edge, NIR, and RGB) using a DJI Phantom 4 Multispectral RTK. The RGB data were analyzed in our other study (Bijou et al., 2023). We used RGB data to generate a digital elevation model for hyperspectral image orthorectification. The main parameters of the UAVs used are shown in Fig. 3.

We used a flight speed of 5 m/s, a flight altitude of 68.9 m, a ground sample distance of 3 cm, and 50 % side-overlap. The flights were conducted between 8 a.m. and 12 p.m. under mostly sunny weather conditions, with occasional fluctuations noted during specific field campaign dates, particularly on June 3 and June 8 due to changing weather conditions (partly cloudy during some phases of the overflight).

2.4. Processing workflow and experimental design

We employed important pre-processing steps (described in chapters 2.5–2.7) and diverse methods to assess the differences in spectra between the two healthy (control) and infested spruce trees (chapter 2.8). As the trees in groups G1, G2, and G3 were infested on clearly distinct dates (see chapter 2.1), we analyzed each group separately to avoid mixing trees at different stages of damage and to ensure consistency in spectral responses. Fig. 4 provides the workflow of the collected data preprocessing and analysis.

2.5. Pre-processing of UAV data

After completing the UAV flights, the collected hyperspectral cubes were subjected to standard pre-processing, including radiometric calibration, atmospheric correction, and geometric alignment. Geometric and radiometric corrections were carried out using Headwall SpectralView software (Červená et al., 2020). Radiometric correction was based on factory-calibrated files and a portable 3 × 3 m fabric target (type 822, Group 8 Technology, Inc., Provo, UT, USA), which was placed within the scanned area during the flights. The calibrated tarp is divided into three sections, each with a known reflectance value (56 %, 32 %, and 11 %), and serves as the basis for the radiometric correction. We converted the data to radiance using the calibration files, and an average radiance spectrum was obtained from the tarp. The known absolute reflectance curves of the tarp panels were then used to scale the radiance values, ensuring a standardised correction process for the entire flight (Angel et al., 2020; Červená et al., 2020).

For geometric correction, we merged the hyperspectral cubes into continuous flight line sequences using GNSS/IMU data recorded during the flights. The digital elevation model generated from the point cloud of the Phantom 4 Multispectral RTK was used to orthorectify the hyperspectral flight lines. RGB and multispectral orthomosaics, along with digital elevation models, were produced in Agisoft Metashape Professional v1.7.2 (Agisoft LLC, St. Petersburg, Russia) from the multispectral imagery. More details on the RGB and multispectral pre-processing procedures are available in Bijou et al. (2023). Mosaicking of the orthorectified hyperspectral flight lines was attempted in QGIS using ground control points as tiepoints and the RGB orthomosaic as a reference image. However, due to challenges in the forested environment, a complete mosaic of the study area for all dates could not be created. Therefore, we focused our analysis on individual flight lines.

Given the importance of radiometric stability for the analysis of multitemporal UAV imagery, we assessed the spectral fidelity and performance of the Headwall Nano-Hyperspec sensor before continuing with further analyses (see Appendix B). To reduce noise and smooth the reflectance spectra, a Savitzky-Golay filter was applied, improving the interpretability of the hyperspectral signal (further details in Appendix C).

2.6. Removal of background and delineation

To isolate the forest canopy and remove the background, for a better and guided manual delineation of tree crowns, each hyperspectral cube was classified using K-means unsupervised classification with a change threshold of 0.5 % and a maximum of two iterations. Increasing the number of iterations to eight did not improve the results. Eight clusters/classes were generated, as this number provided the best separation between canopy (1 class) and background (7 classes). To further refine the resulting mask, particularly in areas where unsupervised classification struggled with background and shadowed pixels, we applied a red band thresholding technique (band 184) following Clark et al. (2005). Pixels with reflectance values higher than the mean tree reflectance in this band were retained to produce a binary forest mask (Dalponte et al., 2014). Individual tree crowns were manually delineated from the hyperspectral cubes in ENVI 5.5, using the created mask and validated with coordinates of trees measured with the total station. Only well-lit and clearly visible portions of the crowns were selected for further analysis.

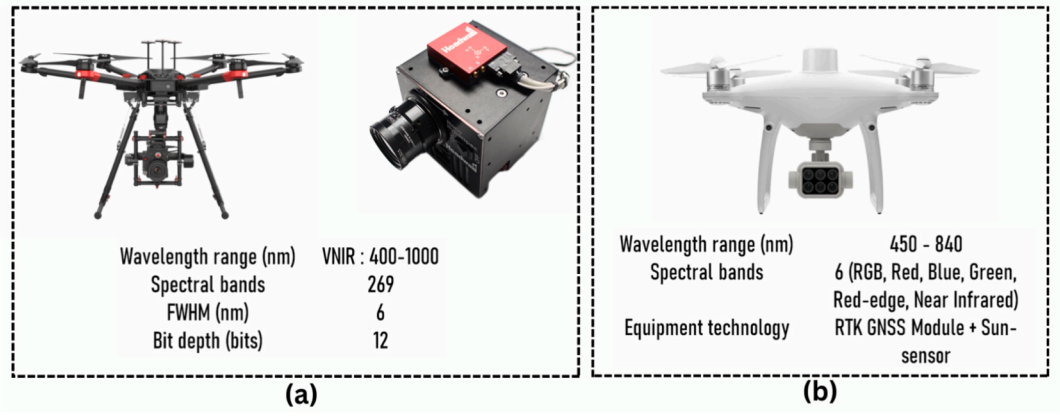

Fig. 3. UAV systems used for data collection over our study area, (a) The DJI Matrice 600 with Nano Hyperspec sensor and the sensor characteristics, (b) Phantom 4 Multispectral RTK UAV system and its characteristics.

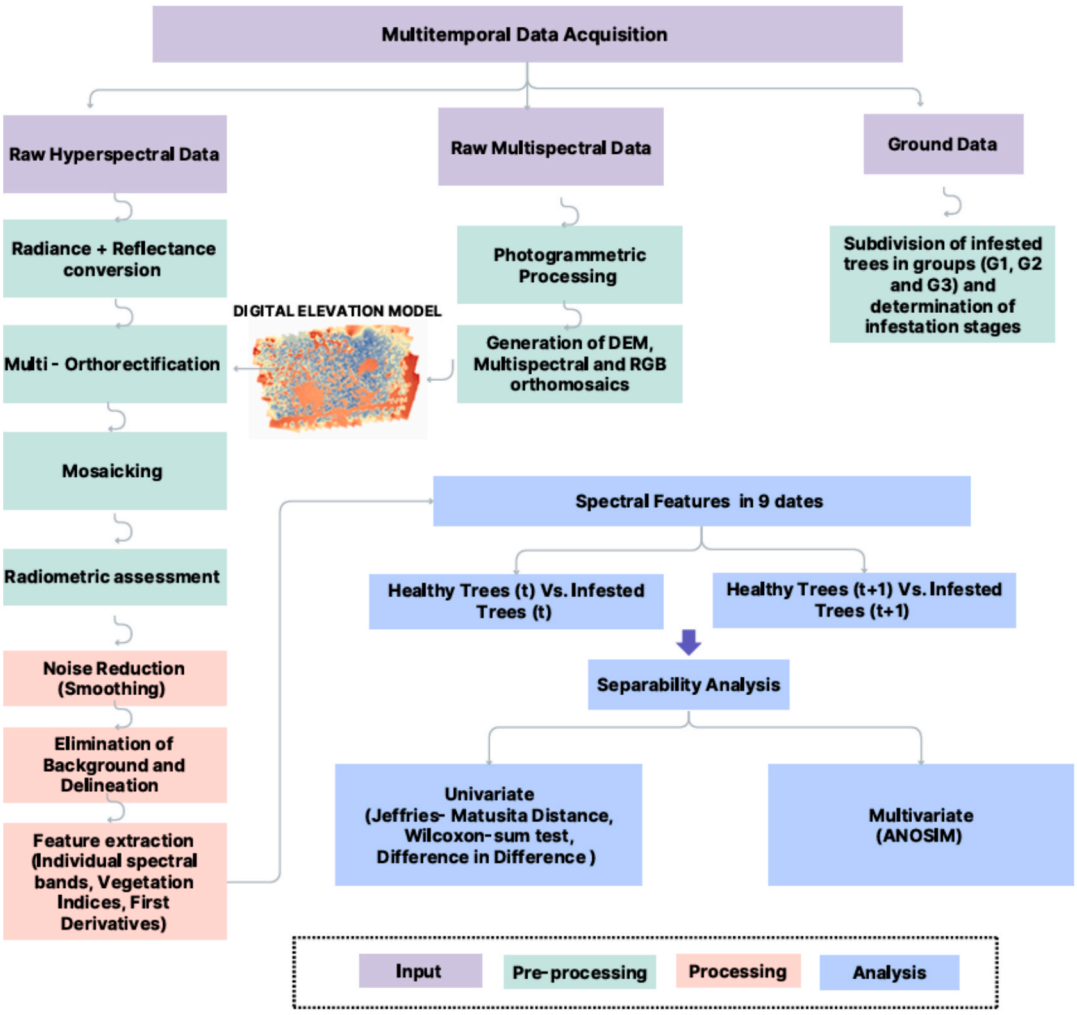

Fig. 4. The workflow of the study, illustrating the progression from data acquisition through preprocessing and analysis. (*Vs: Versus*).

2.7. Feature extraction

As already stated, our analysis focused on the comparison of 23 infested trees subdivided into three groups (G1, G2, and G3) consisting of 11, 6, and 6 trees, respectively, and 23 healthy (control) trees (subdivided into three groups with the same number of trees). We analysed hyperspectral features of both healthy and infested trees during each of 9 sensing periods. These features included: (1) the computed average spectral reflectance for each band (B1–B269) within every delineated tree crown; (2) 25 spectral VIs (see Appendix D); and (3) first spectral derivatives. Derivative analysis is particularly valuable in this context for several reasons. It helps to highlight changes or features in the spectral data that may be subtle or difficult to detect in the original reflectance spectrum. It also sharpens spectral peaks, making it easier to distinguish their positions. Moreover, derivatives are less affected by variations in illumination conditions, which make them more robust for time series analysis (Einzmann et al., 2021; Campbell et al., 2004). We computed the first derivative for both healthy and infested trees for all 9 dates to capture how rapidly the spectral reflectance changes between consecutive wavelengths. The following formula was used for the calculation of the first derivatives:

$$\frac{dR_{\lambda(i)}}{d\lambda_i} = \frac{R_{\lambda(i+1)} - R_{\lambda(i-1)}}{\lambda_{i+1} - \lambda_{i-1}}$$

where, R is the spectral reflectance at a given wavelength, dR is the change in reflectance between two adjacent bands. dλ is the difference in wavelength between those bands.

2.8. Statistical analysis of spectral separability

To evaluate the spectral separability between healthy and infested trees, we conducted four types of statistical analyses: Jeffries-Matusita (JM) distance, Analysis of Similarities (ANOSIM), Wilcoxon rank-sum test (WRST), and Difference-in-Differences (DiD). Table1 summarizes which method was applied to which type of the spectral features and group of infested trees. Although all statistical methods were initially tested across various spectral features and tree groups, we focus here on

Table 1
Statistical methods used for analyzing spectral features and groups of infested trees for each of the infestation groups. The symbol "+" indicates that a method was applied, while "–" indicates that the method was not used.

Statistical method		JM	ANOSIM	WRST	DiD
Spectral features	Reflectance	+	+	+	+
	1st derivatives	–	+	–	–
	VIs	–	–	+	+
Groups of Infested trees	G1 (11 trees)	+	+	+	+
	G2 (6 trees)	+	+	+	–
	G3 (6 trees)	+	+	+	–

Note: JM: Jeffries Matusita distance, WRST: Wilcoxon rank-sum test, ANOSIM: Analysis of Similarities, DiD: Difference in Difference.

the most relevant combinations to avoid redundancy, as raw reflectance, VIs, and first derivatives often share overlapping information. Due to sample size limitations, some analyses were only performed for group G1, which provided a sufficiently large sample for reliable statistical assessment. We used JM and WRST for relative comparisons between the 2 categories, healthy and infested trees, for each sensing date, and DiD method for multitemporal analysis of the 2 categories, leveraging panel data to mitigate heterogeneity and increase sample size. ANOSIM was used as a multivariate approach to assess spectral separability. More details are provided below.

1. The Jeffries-Matusita distance (JM) is a statistical measure commonly employed in the context of spectral feature space in hyperspectral applications (Borges et al., 2007; Padma and Sanjeevi, 2014). In RS, it is used to quantify the separability between two probability distributions, typically representing two different classes in classification problems, and is also used as a feature ranking tool in machine learning (Sen et al., 2019). We calculated JM between healthy and infested trees in particular groups (G1, G2 and G3), across all 269 spectral bands. A JM distance above 1.90 indicates greater separability between two categories, while values below 1 suggest low distinguishability. The JM distance is asymptotic to 2, where 2 suggests complete separability
2. Analysis of Similarities (ANOSIM) is a non-parametric multivariate statistical test used to evaluate whether two or more groups differ significantly based on a dissimilarity matrix. It is commonly employed in ecological and biological research, where the input data represent pairwise dissimilarities between samples (e.g., between species) (Mcilwaine et al., 2019). The dissimilarity matrix quantifies the differences between all sample pairs, typically using Euclidean distance. ANOSIM ranks these distances and computes the R statistic, which quantifies the degree of separation between groups. The R value ranges from –1 to 1, where 1 indicates complete dissimilarity, 0 indicates no difference, and –1 indicates complete similarity. A corresponding p-value is used to determine the statistical significance of the observed differences. We computed the dissimilarity matrix by comparing all pairwise combinations of healthy and infested trees based on their reflectance or first derivatives across all spectral bands. The analysis was performed using the “free” permutation type with 999 permutations. We interpreted the R statistic using three threshold ranges to assess the strength of category separation: $R < 0.3$ (weak separation), $0.3 < R < 0.65$ (moderate separation), and $R > 0.65$ (strong separation). A p-value threshold of 0.005 was applied to assess statistical significance, where p-values below this threshold indicated significant differences between categories
3. The Wilcoxon Rank-Sum test (WRST) is a non-parametric statistical test used to compare two independent groups when the assumption of normality is not met (Wilcoxon, 1945). We employed WRST independently for each sensing period, in order to identify spectral bands and VIs that significantly differed between healthy and infested trees (G1, G2 and G3). Prior to testing, the normality of all 269 spectral bands and 25 VIs was assessed using the Shapiro-Wilk test. As the data did not meet the assumption of normality, we proceeded with the nonparametric WRST. The WRST test offers several advantages: (1) it can be used with non-normally distributed data, (2) it is resistant to outliers because it relies on ranks rather than original measurements, (3) it is suitable for small sample sizes, (4) it is easy to understand and requires minimal statistical knowledge (Dao, 2022). Different significance thresholds were applied depending on the type of data. For reflectance values, which are more prone to variability due to sensor noise and environmental conditions, we used a significance level of 0.05 to allow the detection of meaningful differences while minimizing false negatives. For VIs, which are inherently smoothed and less noisy, a stricter threshold of 0.01 was applied to reduce false positives and ensure greater confidence in the results
4. Difference-in-Differences (DiD) is a quasi-experimental econometric method used to estimate the causal effect of a treatment or intervention by comparing changes in outcomes over time between a treatment group and a control group (Angrist et al., 1999). The fundamental assumption is that, in the absence of treatment, the difference in outcomes between two groups would remain constant over time. By comparing the pre-treatment and post-treatment outcomes for both groups, DiD isolates the effect of the treatment, controlling for any underlying trends or external factors that might influence the outcome. This allows for a causal inference about the treatment’s effect. Although originally developed for use in economics, DiD has since gained traction in environmental, climate, and few RS studies (Fu et al., 2022; Xie et al., 2022; Wang et al., 2021)

We used DiD to assess how the bark beetle infestation (the “treatment”) affects the spectral reflectance in trees over time (within the 9 sensing dates). We divided the trees into two categories: (1) treatment category – trees that have been infested (3rd June for G1) and (2) control category – healthy trees that were not infested. The data includes repeated measurements of reflectance for each tree at nine time points, for the analysis of how the spectral reflectance of the trees changed over time before and after the infestation occurred. We used panel data (or longitudinal data) which refers to observations collected from the same trees over multiple time points. This type of data structure combines cross-sectional data (observations from multiple trees, both healthy and infested) with time series data (repeated measurements over time). We monitored 11 trees, collecting data over 9 time points, which constitutes a panel dataset. Each observation includes: A unit (tree ID or number), a time point (ranging from 1 to 9), a status variable ($1 =$ infested, $0 =$ healthy), and several features (spectral bands and vegetation indices). Panel data structure is beneficial for this study for several reasons. First, it allows for examining the temporal evolution of spectral reflectance across 9 time points, helping to isolate the effects of bark beetle infestation while controlling for general time trends like seasonal changes. Second, panel data enables control for unobserved heterogeneity by accounting for individual tree characteristics that could influence spectral reflectance but remain constant over time. Third, it strengthens causal inference by using both cross-sectional and temporal variation, providing more accurate comparisons between treatment and control categories.

Since infestation (the “treatment”) occurred at different time points, we adopted a heterogeneous DiD framework with the Augmented Inverse Probability Weighting (AIPW) estimator (Callaway and Sant’Anna, 2021). This estimator offers double robustness, reducing potential bias even when some model assumptions are violated. The dataset consisted of 11 healthy and 11 infested trees (for G1), observed at 9 time points, resulting in 198 total observations (22 trees $\times$ 9 dates). We focused on estimating the Average Treatment Effect on the Treated (ATET) for each cohort and time period, represented by dates D1 through D9. In our analysis, two cohorts were identified using a dataset comprising 198 observations, evenly split between the control category (99 observations) and the treatment category (99 observations). The control category includes observations coded as 0, indicating trees that were never treated (i.e. remained healthy), while the treatment category includes observations coded as 1, corresponding to trees that belong to one of the infested cohorts. The ATET reflects the estimated change in the outcome variable attributable to the treatment, relative to the control group, for a given cohort and time period. Each ATET estimate is accompanied by its standard error, z-value, and p-value, enabling statistical inference regarding the significance of the observed effects. Additionally, 95 % confidence intervals are reported for each ATET, representing the range within which the true effect is estimated to lie with 95 % confidence.

Comparing various methods was essential for addressing the unique

temporal and spectral characteristics of hyperspectral data and for cross-verifying results to enhance confidence in the analysis. JM, WRST and ANOSIM were performed using the R programming language (R Core Team, 2023). DiD was conducted in Stata 18 (StataCorp. 2023).

3. Results

In the main body of the paper, we present detailed results (descriptive and statistical), including figures, only for G1 (except for chapter 3.1). For G2 and G3, which represent additional waves of infestation by parental beetles from the initial swarming event with specific developmental patterns and smaller sample sizes, only basic results are mentioned in the main body, and the corresponding outputs are provided in the appendices.

3.1. Development of the bark beetle infestation in the field

The infestation development for trees in groups G1, G2, and G3 (refer to chapter 2.1) is illustrated in Fig. 5. Visible symptoms on the bark (boring holes and resin flow) first appeared on June 3 for G1 (11 trees), on June 15 for G2 (6 trees), and on June 24 for G3 (6 trees). Trees in G1, which were infested earliest, remained longer in the green and yellow crown stages. In contrast, G2 and G3 progressed more rapidly towards the yellow and red stages, with shorter durations in the green stage. By August 25, most infested trees across all groups exhibited complete crown greying, advanced defoliation, and substantial bark loss. While individual trees showed some variation, the described symptom progression reflects the predominant pattern within each group.

3.2. Temporal changes in spectral features

3.2.1. Temporal changes in individual bands (reflectance and 1st derivatives)

The mean spectral signatures, depicting the spectral behavior of G1 infested and healthy trees across multiple sensing dates, are shown in Fig. 6. In the early stages of infestation (up to D4), the spectral characteristics of both healthy and infested trees were largely similar, with some differences observed on June 3 (D2) and June 8 (D3), which were not consistent over time. **A more pronounced divergence became evident only later, particularly on July 19 (D7)**, when reflectance in the red wavelengths noticeably increased and reflectance in the NIR region decreased in infested trees. At this point, however, crown damage was already clearly visible through standard field observation, suggesting that spectral detection occurred relatively late in the progression. In August, these spectral trends further intensified. The mean spectral signatures of G2 and G3 for each date (D1 to D9) are presented in the Appendix E – Fig. E1. For G2, bark beetle stress became evident on D8 (August 4th) with a drop in NIR and a rise in visible reflectance. For G3, a similar shift occurred from D8, marking the onset of significant spectral differences.

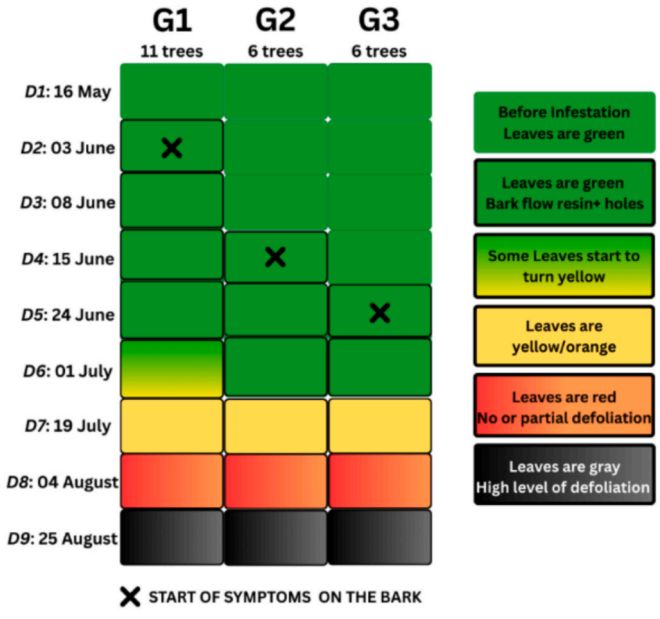

Fig. 5. Bark beetle infestation development observed in the field on the dates of UAV data acquisition for G1 (trees infested on 03 June), G2 (trees newly infested on 15 June), and G3 (trees newly infested on 24 June).

The mean values of first derivatives showed a smooth and gradual progression over time (Fig. 7). Some irregular or abrupt shifts between the healthy and G1 of infested trees were observed on D3 in the red-edge region (700–750 nm), similar to patterns seen in the non-derivative spectra. **The most distinct differences began to appear from D5** within the same spectral range (700–750 nm), and became more widespread by D7, extending across nearly the entire spectrum, with particularly pronounced differences in the 700–750 nm and 480–570 nm regions, indicative of developing bark beetle damage. The temporal analysis of G2 and G3 (Appendix E – Fig. E2) also highlights key spectral regions with notable differences over time, especially in the 480–570 nm and 700–750 nm ranges. The most substantial variations became apparent from D8 (August 4) onward.

3.2.2. Temporal changes in vegetation indices

The rate of change varied among the VIs, with some indices exhibiting greater temporal fluctuations in value ranges than others. In Appendix F – Fig. F1, the radar plots illustrate how infestation influences the spectral response of Vis of infested trees (G1) over time in comparison to healthy trees. A noticeable reduction in overlap of polygons (representing values) between healthy and infested trees was observed from **D4 onwards for several VIs, particularly ARI1, CHLRE, PRI, DDI, CI, CI-G, CI-REG, NR1, and NR2**. For other indices: NDVI, WBI, PSRI, WBI/NDVI, GREENNESS, and ZM the degree of overlap between healthy and infested trees began to decline from D7 (July 19). For the other indices it was even later.

Fig. 8 illustrates the temporal evolution of mean REIP (Red-Edge Inflection Point) shifts between the healthy and G1 of infested trees. **The REIP shift became distinctly discernible on D4 (June 15)**. The pronounced change in the REIP magnitude in this and following dates clearly indicates stress induced by the bark beetle, implying severe damage of the infested spruce trees. The results of G2 and G3 are presented in Appendix F – Fig. F2.

3.3. Statistical analysis of spectral separability

3.3.1. Jeffries-Matusita distance

The separability between healthy and G1 infested trees is presented in a heatmap of the Jeffries–Matusita (JM) distance, based on single-date hyperspectral imagery (Fig. 9). Temporally, the JM distance gradually increased over time, signaling a growing distinction between healthy and infested trees, even without reaching statistical significance. This increase was first observed in the red band, followed by the visible bands, and then the NIR.

For Groups G2 and G3, the most pronounced differentiation was observed on D8 (August 4), as shown in Appendix G – Fig. G1. However, despite these trends, JM distances never exceeded 1.90 for any group or date. Since a JM value of 1.90 or greater is considered indicative of effective separation of healthy and infested trees, and values at or below 1.0 reflect poor separability, the results indicate that the distinction between healthy and infested trees remained limited throughout the study period.

3.3.2. Analysis of similarities

The results of the ANOSIM analysis conducted on both reflectance

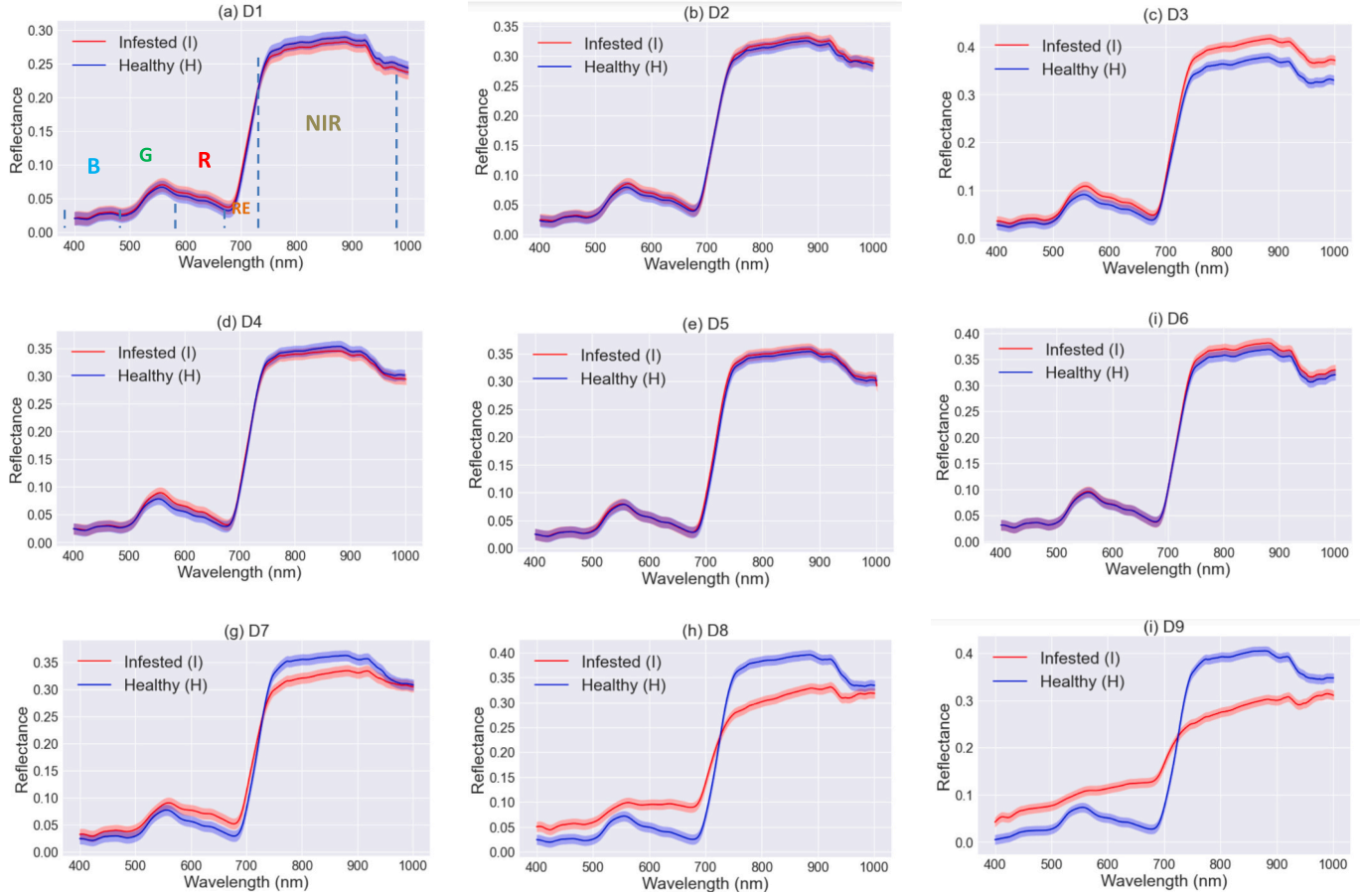

Fig. 6. Mean spectral signatures extracted for healthy trees and G1 of infested trees in each of the 9 sensing dates (D1 – 16 May, D2 – 03 June, D3 – 08 June, D4 – 15 June, D5 – 24 June, D6 – 01 July, D7 – 19 July, D8 – 04 August, D9 – 25 August); (a) shows the spectral regions: Near infrared (NIR), RedEdge (RE), Red(R), Green (G), Blue (B). (For interpretation of the references to color in this figure legend, the reader is referred to the web version of this article.)

spectra and their first derivatives for G1 are presented in Table 2. For reflectance, the R values remained below 0.3 until D7 (July 19), indicating minimal separability between the healthy and infested trees. On D8 (August 4), R values increased to the intermediate range ($0.3 < R < 0.65$), and by D9 (August 25), they exceeded 0.65 suggesting strong separation at this final stage. In contrast, the first derivatives revealed differences earlier. For G1, R values were already in the intermediate range by D7 and surpassed 0.65 on D8, indicating earlier spectral divergence between healthy and infested trees than reflectance alone could detect. **Notably, for G1, discernible differences emerged on D8 using reflectance, and as early as D6 (July 1) based on first derivatives, and demonstrating greater sensitivity of this approach (with $0.3 < R < 0.65$ and p-value < 0,005).**

Similar patterns were observed in G2 and G3, as shown in Appendix H – Fig. H1. Both groups exhibited R values below 0.3 before and shortly after infestation. In G2, the transition to values above 0.65 occurred on D8 (August 4), while in G3, R values remained below 0.3 until D7, shifted into the intermediate range on D8, and exceeded 0.65 only on D9 (August 25). Overall, the ANOSIM analysis based on individual bands with p-values < 0.005 decisively rejects the null hypothesis for group separation from D8 onward for G1 and from D9 for G2 and G3. The results confirm that first derivatives are more sensitive for the detection of spectral differences associated with bark beetle infestation.

3.3.3. *Wilcoxon rank-sum test*

The heatmaps in Fig. 10 illustrate the p-values obtained from the Wilcoxon rank-sum test, used to assess the spectral separability between healthy and G1 of infested trees for each sensing date. For individual **spectral bands, significant differences (p-value < 0.05) between healthy and infested trees were first observed on D4 (June 15th, 13 days after infestation on the bark** was first detected), particularly **within the 692–706 nm range**. This pattern extended on D5 (June 24th) to the same range and additionally to 626–644 nm. By D6 (July 1st), significant differences spanned a broader portion of the spectrum, from 567 to 715 nm. On D7 (July 19th), disparities were primarily concentrated in the visible range. These effects intensified on D8 (August 4th), with significant differences expanding into both the visible and near-infrared (NIR) regions. By D9 (August 25th), significant separability was observed across nearly the entire spectrum, except for some bands within the red-edge region. **For VIs, noticeable separability (p-value < 0.01) began on D4 (June 15th)**, with significant differences observed for indices such as **PRI, CHLRE, RENDVI, DATT, MRESR, NDRE, DDI, CI-REG, REIP, and ZM**. Results for G2 and G3 are in Appendix I – Fig. I1. In G2, statistically significant differences became evident on D8 (August 4th, 49 days after detected infestation), particularly within the visible and NIR plateau regions. Similarly, in G3, significant spectral differences began to appear on D8 (August 4th), initially within the visible spectrum and expanding to include both visible and NIR wavelengths by D9 (August 25th). In terms of VIs, separability in G2 emerged by D8, and G3 exhibited comparable trends to G2.

3.3.4. *Difference in difference*

The results of the DiD analysis for comparison of reflectance of healthy and G1 of infested trees revealed the following findings across the nine time periods and individual spectral bands (see Fig. 11), listed

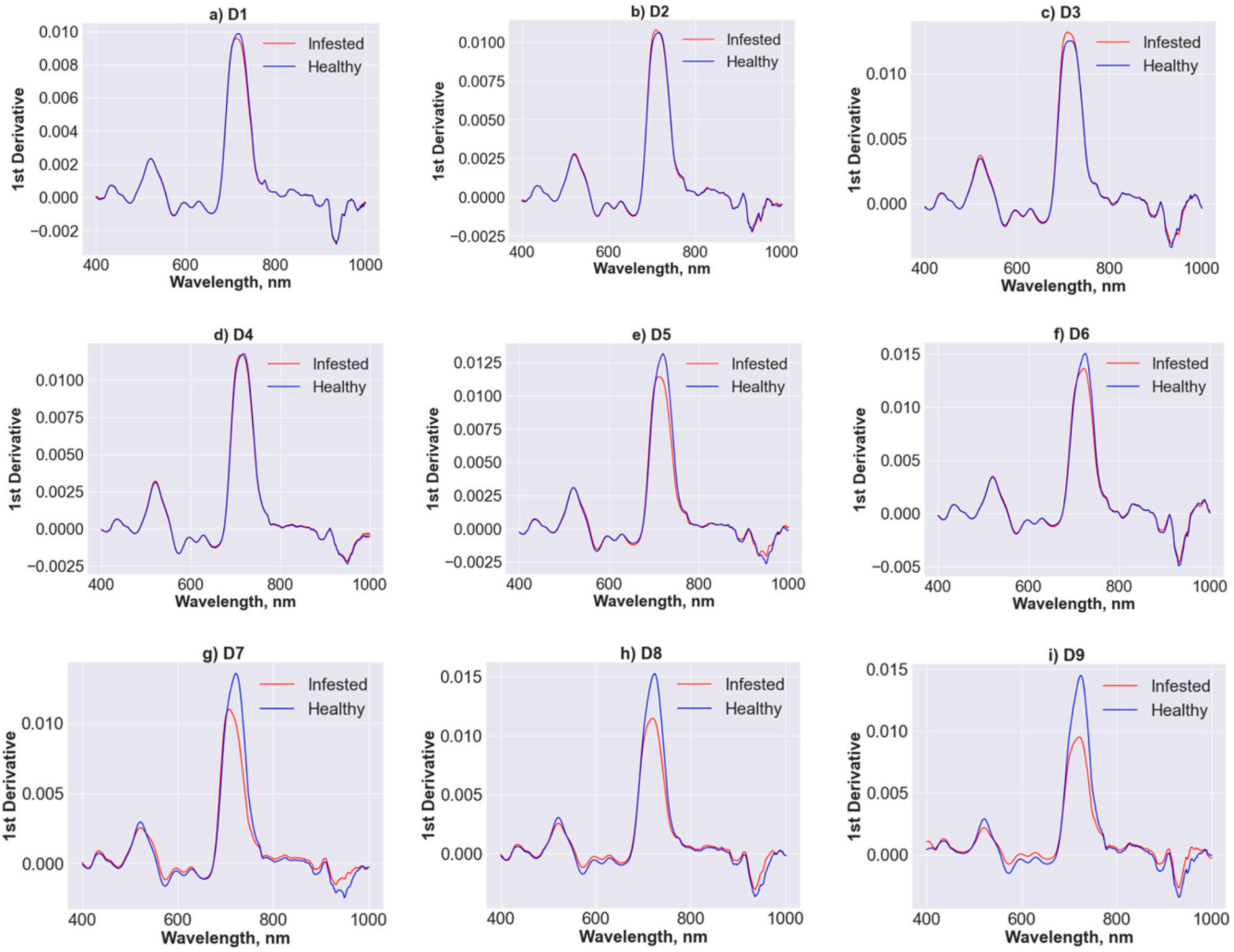

Fig. 7. 1st derivative mean values for healthy trees and G1 of infested trees in each of the 9 sensing dates (From D1 – 16 May 2022 to D9 – 25 August 2022).

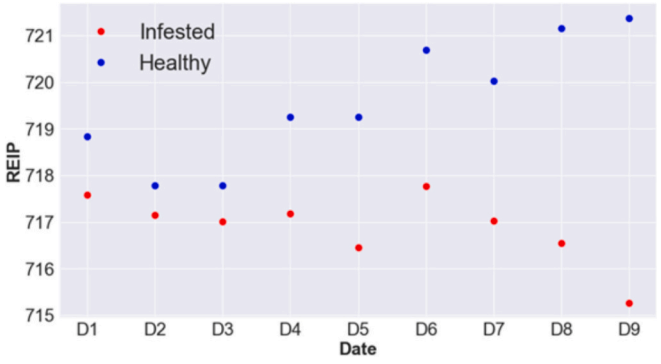

Fig. 8. REIP temporal evolution of the comparison between healthy trees and G1 of infested trees in each of the 9 sensing dates (From D1 – 16 May 2022 to D9 – 25 August 2022). (*Note:* This visual representation of REIP was selected for its interpretability, as VIs and REIP have significantly different ranges.). *REIP: Red-Edge Inflection Point.* (For interpretation of the references to color in this figure legend, the reader is referred to the web version of this article.)

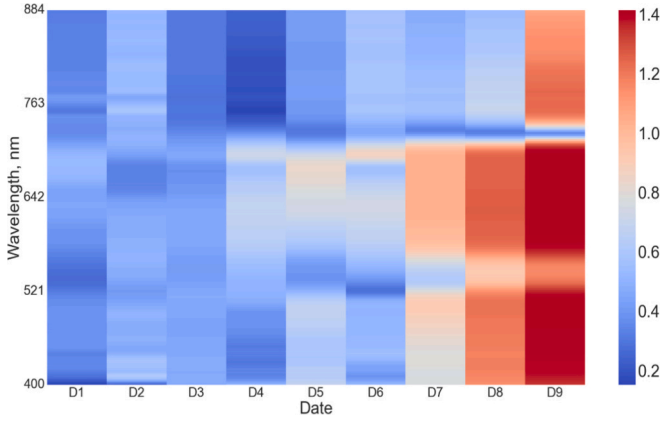

Fig. 9. Heatmap of bands importance using Jeffries-Matusita Distance computed between healthy and G1 of infested trees for each of the 269 spectral bands and for each of the 9 dates of acquisition (From D1 – 16 May 2022 to D9 – 25 August 2022).

in chronological order:

- At D6, spectral bands B134 to B138 (697–706 nm) showed significant differences, with a positive treatment effect.
- From D7 onwards, significance appeared in bands B4 to B133 (406–695 nm), consistently demonstrating a positive treatment effect.

Table 2
Results of ANOSIM between healthy trees and G1 of infested trees (for Reflectance and 1st derivatives) for each sensing date, R values and p-values for G1; light orange cells highlight R < 0.30, orange cells highlight 0.30 < R < 0.65, and red cells highlights R > 0.65.

Day (date)	Reflectance		1st derivatives	
	R	P-value	R	P-value
D1 (16 May)	0.02494	0.583	0.06912	0.105
D2 (03 June)	0.01863	0.267	0.03967	0.191
D3 (08 June)	0.02585	0.580	0.007363	0.317
D4 (15 June)	0.03286	0.265	0.0846	0.089
D5 (24 June)	0.06687	0.132	0.2727	0.006
D6 (01 July)	0.05545	0.128	0.3351	**0.001**
D7 (19 July)	0.2066	0.021	0.492	**0.001**
D8 (04 August)	0.361	**0.003**	0.765	**0.001**
D9 (25 August)	0.8656	**0.001**	0.996	**0.001**

- Starting from D8, spectral bands B148 to B233 (729–919 nm) exhibited significant differences, but with a negative treatment effect.
- Finally, significance persisted in bands B234 to B243 (922–942 nm) until D9, continuing to show a negative treatment effect.

Regarding VIs, significant effects were observed at various time points, as illustrated in Fig. 12:

- At D5 (24th June), the indices REIP, MRSER, and PRI showed significant differences ($p < 0.05$), all indicating a negative treatment effect.
- At D6 (1st July), significance was detected for a broader set of indices: CI_REG, CI, DDI, DATT, NDRE, RENDVI, CHLRE, NR1, NR2, ZM, and ARI1.
- At D7 (19th July), the first significant differences appeared for NDVI, PHYT, N_NDVI, CI_G, GREENESS, CARI, WBI/NDVI, and PSRI.
- At D8 (4th August), significance emerged for the MCARI index.
- Finally, the index CARI did not exhibit statistical significance until the last time point, D9 (25th August).

A similar trend in significance was observed earlier for both reflectance and VIs. At D4, a positive treatment effect was detected in spectral bands B51 to B87 (511–592 nm), and for several VIs at D2 (June 3rd), including PHYT, N_NDVI, DATT, MRSER, RENDVI, GREENESS, CHLRE, ARI1, PSRI, NDVI, NR1, NR2, and ZM. However, this significance was not consistent over time.

4. Discussion

4.1. Important findings and their comparison with previous studies

In our study, we were able to detect bark beetle infestation in the hyperspectral imagery for G1 of infested trees on June 15, which is day

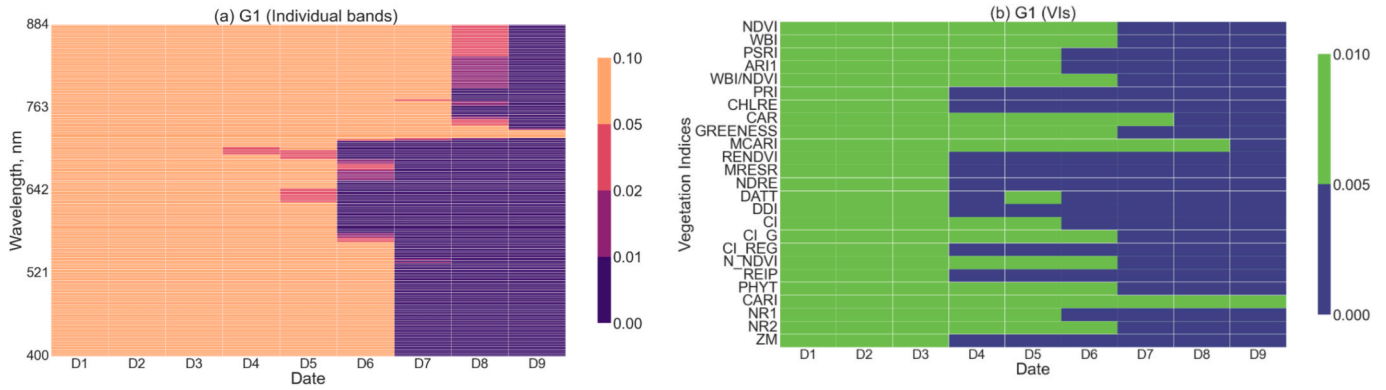

Fig. 10. P-values heatmaps results of the spectral separability between healthy trees and G1 of infested trees for each sensing date (From D1 – 16 May 2022 to D9 – 25 August 2022), (a) for individual bands and (b) VIs.

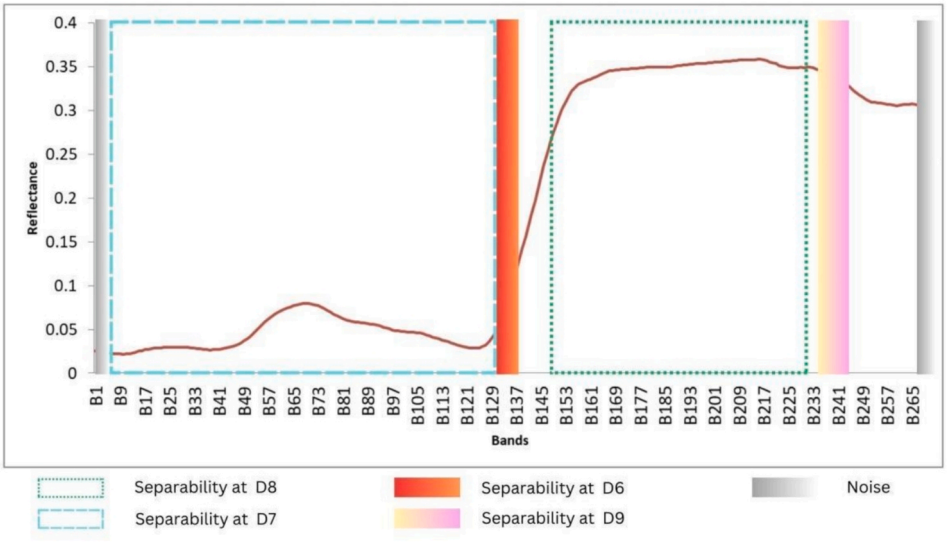

Fig. 11. Spectral regions with significant differences detected by the DiD method at different sensing dates.

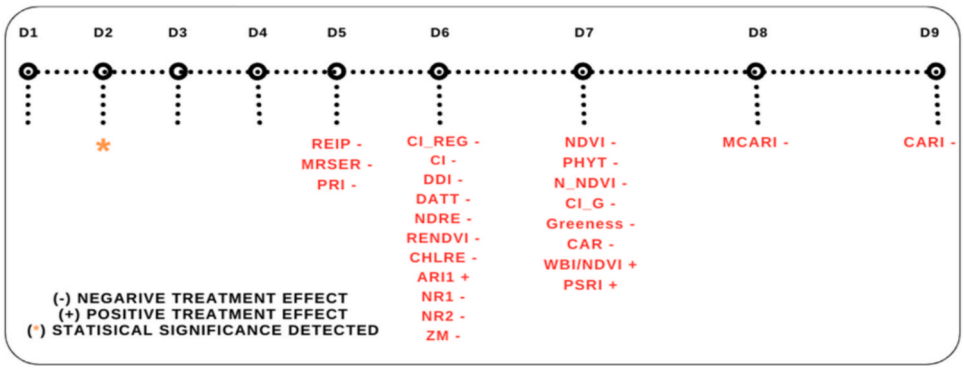

Fig. 12. Significant differences detected by the DiD method for VIs observed at nine dates for G1. The asterix refers to the statistical significance observed for several VIs as well, at D2 (June 3rd), including PHYT, N_NDVI, DATT, MRSER, RENDVI, GREENESS, CHLRE, ARI1, PSRI, NDVI, NR1, NR2, and ZM, which was not consistent over time.

13 after the first visible bark symptoms (such as boring holes, boring dust and resin flow), appeared on the trunks of infested trees. On this day, we identified statistically significant differences between healthy and G1 of infested trees using the WRST (refer to Fig. 10). This was approximately 22 days after the estimated start of bark beetle infestation on May 24, as indicated by thermal sum calculations. The detection occurred while the trees were still in an early GS, 15 days before any visible crown discoloration.

Compared to previous studies, our detection timing is rather early. Huo et al. (2023a) reported detectable spectral symptoms 35 days post-attack, Bozzini et al. (2024) approximately two months post-attack, and Bárta et al. (2022) 23 days after the first visible bark symptoms. The difference may be due to the lower spatial resolution of aerial hyperspectral imagery (0.5 m) used by Bárta et al., in contrast to our UAV-based imagery at 3 cm resolution. In pine species, specifically *Pinus thunbergii* infested by *Bursaphelenchus xylophilus*, Pan et al. (2024) observed spectral changes 14 days post-infection using close-range spectroscopy and a Random Forest classifier (accuracy 59.2 %). However, the mechanism of damage in pine wilt disease differs from that in spruce trees attacked by bark beetles (Umebayashi et al., 2011; Urbanek Krajnc, 2009), which likely accounts for the variability in detection timing between species.

The most effective spectral wavelengths for early detection in our study were located in the red-edge region (692–706 nm), followed by the red region (626–644 nm), the broader green–red–red-edge region (568–715 nm), and finally the NIR region (740–956 nm). Notably, the interval between 720–729 nm appeared insensitive to infestation. These findings are consistent with previous studies identifying red-edge reflectance, especially around 705 nm, as the earliest spectral indicator of infestation (Huo et al., 2023a). Huo et al. (2023a) also reported red-edge sensitivity. Their detection occurred later, 15 % of trees were detected at 35 days post-attack (June 21), and 90 % after 70 days, when discoloration became visible. In their follow-up study (Huo et al., 2024), spectral differences between healthy and infested trees were again detected in the red-edge region (670–780 nm). The effectiveness of the red-edge region has also been confirmed by several other studies (Minařík and Langhammer, 2016; Hellwig et al., 2021; Bárta et al., 2021; Abdullah et al., 2019; Einzmann et al., 2021; Campbell et al., 2004). According to Kautz et al. (2024), across 26 reviewed studies, the red-edge had a high potential for detecting GS at 45 %, followed by the green region (40.9 %), with lower effectiveness in NIR (36.4 %) and blue (22.7 %) bands across 26 reviewed studies.

In comparison with red-edge, the red region becomes more informative at later stages not only in our case but also in other studies (Klouček et al., 2019; Junttila et al., 2022). Bárta et al. (2022) detected infestation based on red-band differences 23 days after bark symptoms appeared. The limited sensitivity of the NIR region in early infestation stages noted in our study was supported by several others (Bijou et al., 2023; Dalponte et al., 2023; Trubin et al., 2024; Klouček et al., 2019; Bárta et al., 2022; Huo et al., 2021). While red-edge reflectance is highly sensitive to early changes in chlorophyll concentration and photosynthetic efficiency, NIR primarily reflects internal leaf structure and biomass, which are typically affected later. At early stages, these structural changes may be too subtle to impact NIR reflectance significantly. Moreover, NIR signals may be influenced or masked by unrelated factors such as leaf hydration, water stress, or canopy geometry (Barbedo, 2019; Zhang et al., 2023; Hase et al., 2022), further complicating interpretation.

Regarding detection using VIs, red-edge VIs outperformed all others in our study. We observed significant differences between healthy and infested trees in indices such as PRI, CHLRE, RENDVI, MRESR, NDRE, DATT, DDI, CI-REG, REIP, and ZM as early as June 15, i.e. 13 days after visible bark symptoms appeared, similarly to the timing of direct spectral detection (refer to Appendix F – Fig. F1). In Bárta et al. (2022), REIP, PRI, and ANCB650–720 showed the strongest significance 22 days after the first bark symptoms. In contrast, Huo et al. (2024) reported lower detection rates for PRI and REIP (0.69 and 0.34, respectively) in a scenario where beetle swarming occurred later in the season (after July 5).

Indices associated with pigment content, such as NDVI, were found to be less effective during the middle of the season. Their performance improved only later, particularly on July 19 for G1 (which corresponds to 45 days after bark symptoms, 56 days after the start of infestation, and 18 days after start of crown discoloration). In Bozzini et al. (2024), NDVI and SAVI detected infestation 33 days after bark beetle activation, while NDRE, GNDVI, and MR_mDSWI2 showed significant detection 63 days after activation. Similar temporal patterns were also reported by Klouček et al. (2019) and Dalponte et al. (2023).

In our case, NDRE also proved to be an effective index for GS detection, supporting the findings by Bozzini et al. (2024) and Marx et al. (2024), who achieved 77.4 % accuracy in mid-June using the NDRE 758_714 index, despite limited information on the exact timing of infestation. Dalponte et al. (2023) reported a first-generation bark beetle attack after May 6, with bark symptoms in their group G1 observed on July 28, and spectral changes were detected on August 11, using indices such as NDRE, GARI, NDVI, GNDVI, and NRVI, which is in close agreement with our findings.

Based on the consistency of observed differences, we consider D4 (15 June) to be the first reliable detection date in our study, as the spectral and index-based separability between healthy and infested trees remained stable from this point onward during following dates. Some results indicated potential differences already on D3 or even D2, particularly spectral signatures extracted for healthy and infested trees and the results of DiD analysis (see chapters 3.2.1 and 3.3.4). However, the WRST did not identify a statistically significant difference. This result is best explained by increased within-group variability caused by unstable illumination during image acquisition on D2 and D3 (refer to

Section 2.2), when intermittent cloud cover led to a mix of sunlit and shaded crowns. This likely masked real physiological differences by increasing overlap between reflectance distributions.

The WRST, a non-parametric method, compared healthy and infested trees within a single acquisition date, minimizing the impact of environmental variables. Unlike DiD, which is influenced by factors like light conditions and weather, the WRST isolates differences related to tree health, controlling for external variables. On D4, the Wilcoxon test detected spectral differences for G1 by excluding these confounding factors. DiD, in contrast, is more robust for multitemporal analysis but can be affected by seasonal variation or events such as flowering or changes in illumination. This limitation became evident on D2, when DiD indicated significance in some indices. However, this significance cannot be attributed to bark beetle infestation due to the lack of temporal consistency. Among the methods applied, WRST is considered to be most robust against outliers and non-normal distributions, making it the most reliable for detecting true spectral separability under inconsistent acquisition conditions and small sample size (Dao, 2022).

In addition to WRST and DiD, we tested JM distance and ANOSIM approaches to evaluate separability between categories (healthy and infested trees), focusing on interpretable methods suited to our small-scale dataset. These methods were found to be less sensitive for early detection. JM showed low category separability during the early infestation stages, aligning with findings by Magstadt et al. (2021), who observed similar limitations in distinguishing recently stressed trees. ANOSIM was more sensitive applied to first derivatives rather than direct reflectance but still showed limited robustness across spectral regions and time steps.

One important insight from our study is that separating trees infested during different waves of attack by parental beetles from the initial swarming event can improve the detection of early spectral signs of infestation. In our case, the first visible bark symptoms appeared in group G2 12 days after G1, and in group G3 21 days after G1 (i.e. 8 days after the date of successful spectral detection of infestation in G1). Mixing signals from trees already showing developing symptoms (G1), trees that had just been infested (G2), and still healthy trees (G3) could mask the early spectral indicators specific to G1. This temporal separation, suitable mainly in research studies, is not only methodologically justified but also ecologically grounded. *Ips typographus* typically spreads through stands in waves, driven by staggered swarming flights, microclimatic variation, and differences in host tree susceptibility (Jones et al., 2019; 2014, Botterweg 1982). For example, sun-exposed edge trees may be attacked earlier – a pattern described as the "sun effect" (Kautz et al., 2013). Accounting for this spatiotemporal pattern is critical for accurate analysis and interpretation of remote sensing data.

4.2. Possibilities to enhance bark beetle management using remote sensing

Comparison of results from various bark beetle studies and assessments of the effectiveness of RS for early bark beetle detection remains challenging due to multiple factors, including differences in weather conditions, altitude, availability of reliable ground truth data and also time series of RS data with high spectral and spatial resolution. A major issue lies in the lack of standardized definitions, particularly regarding the timing and characterization of infestation stages. Researchers often define the GS, YS, RS and GRS in their studies independently of ground truth observations, phenological stages, and based only on crown discoloration in RGB orthomosaics. They frequently do not provide clear criteria regarding the start and duration of each RS stage in comparison to phenological stages. This lack of clarity is particularly relevant for the GS, as the exact timing of start of infestation is often uncertain or only loosely estimated. In our view, the critical factor is not whether detection occurs during the GS, but how early within this stage it takes place (specifically, before initial crown discoloration and before the emergence of new filial generation of beetles). The subsequent YS, RS and GRS was not the focus of this study, as crown discoloration visible at those points generally indicates that the optimal window for effective sanitation has already passed.

As referred in the Introduction, there have been previous attempts to subdivide the GS, but these efforts were incomplete or lacked consistent criteria (Dalponte et al., 2023, Kautz et al., 2024). In our study, we combined detailed ground truth data (based on repeated field temporal observations of each infested tree), a dense time series of hyperspectral imagery, thermal sum calculation (for the start of swarming estimation), consultations with experienced forestry experts, and an extensive literature review. Based on these inputs, we attempt to estimate the time window within the GS (in connection with the phenological development and progression of bark beetle infestation) during which RS remains effective and can support timely and targeted sanitation efforts.

In our view, the GS should be subdivided more precisely, because towards its end, detection using RS may no longer be early enough to allow for effective sanitation. Therefore, we propose a new subdivision of the GS, illustrated in Fig. 13. The left part of the figure is based on our specific data and observation dates for G1, including Day 13, when we were able to detect the infestation in our spectral data. The right part of the figure presents generalized milestones and key points that indicate the critical time frame for effective RS-based detection. We propose dividing the GS into three sub-stages: G-HS, G-BS, and G-YS, each marked by approximate time intervals of several weeks, representing meaningful thresholds for practical forest management.

We defined the G-HS stage (Green Hidden symptoms Stage) as a period immediately after the estimated start of infestation, when trees have already been infested (according to the result of the thermal sum calculation), but symptoms of bark beetle presence are very subtle and invisible from the ground. Therefore, we call this infestation a "hidden" infestation. This may occur when bark symptoms (tiny entry holes) remain in the upper parts of the crown and boring dust is produced only minimally, making detection from the ground nearly impossible. The estimated duration of this stage in our study is approximately 10 days. Detection by RS at this stage remains uncertain and largely hypothetical, as infested trees most probably do not yet exhibit sufficiently pronounced physiological changes to be detectable in the spectral signal. To our knowledge, evidence of successful detection by RS in this stage has not been reported in the literature.

The subsequent stage, G-BS (Green Bark symptoms Stage), is defined as the period when infestation symptoms become clearly visible on the bark in the lower parts of the trunk, but no discoloration is yet visible in the crown. This stage begins approximately 10 days after infestation (up to two weeks after infestation according to Lubojacký et al., 2018, Webb et al., 2024) and we assume it lasts approximately 3 weeks. During this stage, RS can be an effective tool for detecting the extent of the outbreak and identifying infested trees. We assume that if detection occurs within 3 weeks after bark-visible infestation (i.e., approximately 4–5 weeks from the estimated start of infestation in our case), it is still early enough to prevent the emergence of a new generation of bark beetles (the point of the safe detection – Fig. 13). Detection in this stage can therefore effectively prevent beetle emergence and significantly contribute to rapid sanitation and the prevention of further spread. In our case study, the first reliable detection of the G1 of infested trees occurred during this "safe stage" – on Day 13 after the bark-visible infestation.

Towards the end of the G-BS, around the 4th week after bark-visible infestation (approximately 5–6 weeks from infestation), this may be the last possible moment for RS to detect infestation in a timely manner (the point of the last moment detection). Particularly during strong outbreaks under warm and dry conditions, the emergence of a new beetle generation may already occur during this time (Jacoby et al., 2019, Kautz et al., 2023), meaning that detection may no longer enable effective sanitation.

This is followed by the G-YS (Green-Yellow Stage) characterized by initial crown discoloration (first yellowing mixed with still predominantly green foliage) which starts approx. in week 5 after the bark-visible infestation. This stage is associated with a high probability of

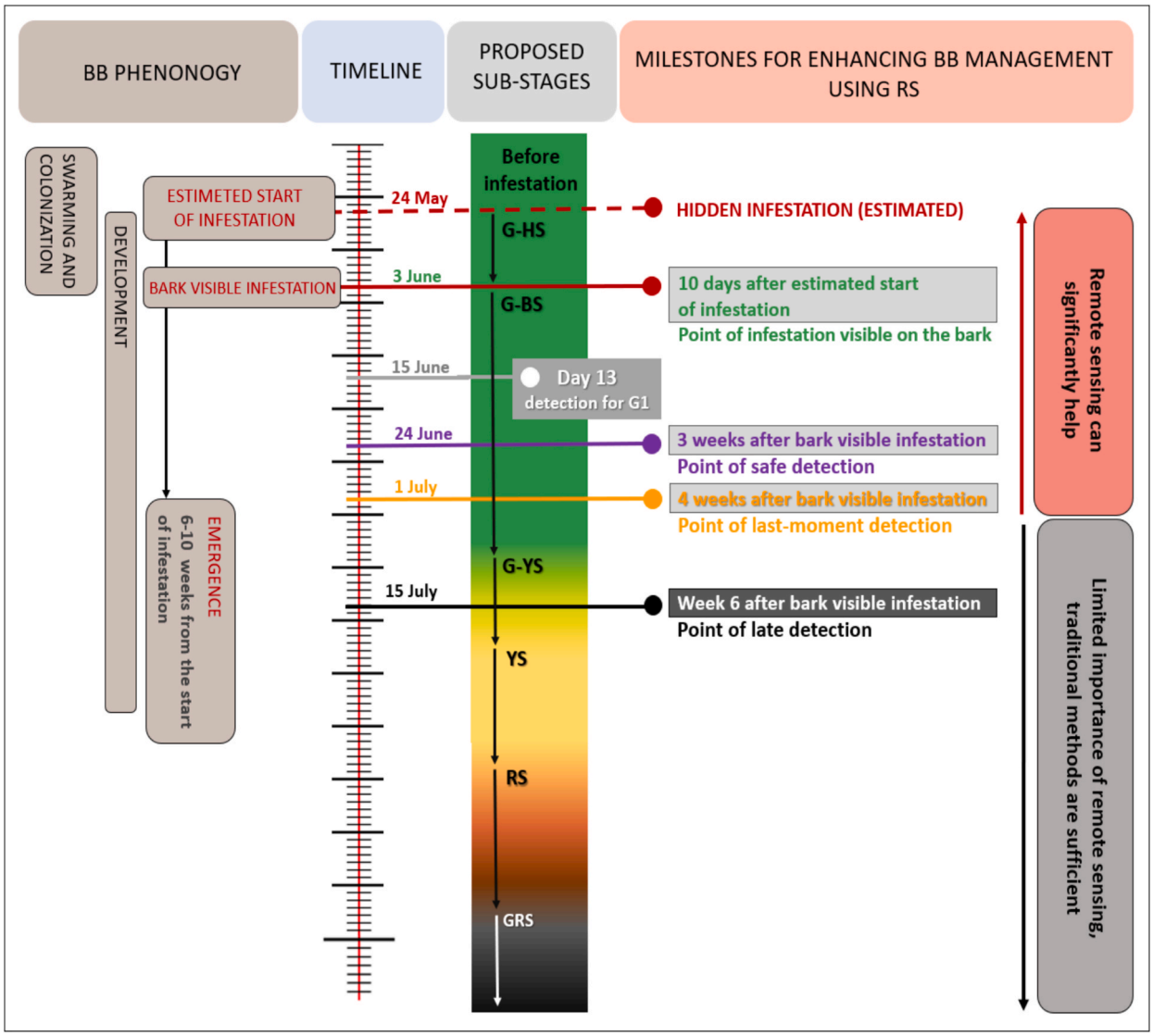

Fig.13. Proposed sub-stages of the green stage and key milestones for the enhancement of bark beetle management using remote sensing, based on our observations for the overwintered generation. The left part of the figure reflects our specific data and observation dates for G1, including Day 13, when we were able to detect the infestation in our spectral data. The right part presents a set of generalized milestones, proposed based on observed infestation dynamics, that indicate the approximate critical time frame for effective remote sensing-based detection, aligned with the timeline of G1 infestation and its phenological development. For a detailed explanation of the individual stages and key points, refer to the text in this chapter (Discussion). *Note: Bark beetle development and emergence were not modelled; the timing is only theoretical.* (For interpretation of the references to color in this figure legend, the reader is referred to the web version of this article.)

second-generation bark beetle emergence, beginning approximately in week 6 after bark-visible infestation (Bárta et al., 2022, Kautz et al.,2023, Kautz et al., 2024). Therefore, week 6 after bark-visible infestation can be considered the starting point of late detection, beyond which preventing the emergence of a second generation is no longer possible. Additionally, since visible yellowing is already apparent at this stage, field detection becomes easier, and the importance of RS decreases significantly. Detection using RS in subsequent stages, YS, RS, and GRS, has rather limited value for forest management, as the infestation is easily recognizable with traditional methods, emergence is already in progress, and intervention is too late to have a significant impact.

The proposed stages of RS detection and key points are derived from our experience, existing publications on RS-based detection, and primarily from bark beetle phenology and the diagnostic importance of field-observed symptoms. We are aware that in reality, the boundaries between these stages are not strict but rather flexible, as they gradually transition into each other. However, in principle, these stages and key milestones should be applicable and relevant for enhancing the effectiveness of RS in bark beetle management in general. Nevertheless, specific conditions of other case studies or areas should always be taken into consideration.

While the proposed early detection method based on UAV sensing and hyperspectral data shows strong potential at the local scale under controlled conditions, its feasibility for larger forested areas remains limited. Achieving high spatial and spectral resolution often results in reduced spatial coverage and increased computational requirements. Hyperspectral sensors are costly and often impractical in field settings. The data processing is complicated by high dimensionality, large data volumes, noise, atmospheric interference, and the difficulty of mosaicking forested areas (Adão et al., 2017). A solution, suggested by Marx et al. (2024), involves resampling hyperspectral data into broadband multispectral data, using resampled NDRE for GS tree classification, with no loss of accuracy between the two sensors. Similarly, Huo et al. (2024) developed green-shoulder indices using hyperspectral data but targeted them for use with simpler, less costly multispectral sensors.

Based on our findings on the effectiveness of the red-edge region (692–706 nm) for early detection, sensors specifically designed to capture this spectral range could be developed. For example, the MAIA S2 multispectral camera (SAL Engineering S.R.L. and EOPTIS S.R.L., Italy), with nine spectral bands covering wavelengths from 390 to 950 nm and used by Huo et al. (2023), could represent a viable alternative to hyperspectral sensors, particularly when high-density imagery and ground-truth data are collected within the first three weeks following the bark visible infestation. However, additional studies are needed to determine whether such multispectral configurations can consistently achieve detection performance comparable to hyperspectral systems, particularly in early infestation stages.

5. Conclusions and future directions

5.1. Conclusions

- In our study, we demonstrated the effectiveness of the time series of UAV hyperspectral imagery in detecting the bark beetle infestation. We were able to detect the infestation 13 days after the visible symptoms of infestation appeared on the lower parts of the bark. It was on June 15–22 days after the estimated start of infestation. The detection occurred while the trees were still in G-BS stage, 15 days before any visible crown discoloration.
- The most effective spectral wavelengths for early detection in our study were located in the red-edge region (692–706 nm) and the most sensitive VIs were PRI, CHLRE, RENDVI, MRESR, NDRE, DATT, DDI, CI-REG, REIP, and ZM. The most sensitive and robust detection method was WRST followed by DiD.
- Hyperspectral data provides enhanced capability for identifying early forest damage caused by bark beetles compared to multispectral data. In our previous investigation using multispectral imagery for the same dates and with the same spatial resolution, significant statistical results did not emerge until a later stage in the season, around July 19th (Bijou et al., 2023), likely due to the coarser spectral resolution.
- We proposed new sub-stages of the GS to improve the timing and targeting of RS-based detection: **G-HS** – **green hidden symptoms** stage with subtle bark symptoms hidden in the upper parts of the trunk (lasts approx. 1–10 days from the start of infestation); **G-BS** – **green** stage with **bark symptoms** on the lower parts of the trunk and crowns remaining green (lasts approx. 3 weeks); **G-YS** – **green-yellow stage** with initial crown discoloration (starts approx. in week 5 after bark visible infestation).
- Our results indicate that RS detection during the late GS, particularly in the late G-BS stage, occurring later than approx. 4 weeks after bark visible infestation, may no longer be timely enough, especially in cases where the emergence of a new bark beetle generation begins within this period.
- We concluded that if RS detection occurs within three weeks after bark-visible infestation, it can serve as a highly effective tool to enhance bark beetle management and prevent further spread of the infestation.

5.2. Future directions and recommendations

- For future research and practical application in the field of remote sensing-based detection of bark beetle infestation, we recommend that studies focusing on early detection use clearly defined and standardized sub-stages of bark beetle infestation, supported by reliable ground-truth data and detailed information on the timing and duration of symptom development in each phenological stage. With such methodological precision will it be possible to robustly demonstrate the ability of remote sensing to detect bark beetle infestation in a timely manner, for an efficient forest sanitation.
- Dense time series of hyperspectral data from the start of infestation, with spatial resolutions on the order of centimeters, are recommended for the effective detection of early-stage bark beetle infestation. This approach currently faces practical limitations, such as high sensor costs, limited spatial coverage, need of an intensive field support, and complex data processing, which constrain its scalability to larger forested areas. Despite these current limitations, our experimental approach represents an important step toward refining early detection methods, which are likely to become increasingly effective and scalable as remote sensing technologies continue to advance.
- Developing selective, low-cost sensors optimized for the most sensitive spectral regions could significantly enhance early detection capabilities and improve operational management practices when combined with UAV platforms capable of efficiently covering large forest areas. In light of our results, the red-edge region appears particularly promising for this purpose and deserves further exploration.

Declaration of generative AI and AI-assisted technologies in the writing process

During the preparation of this work the authors used ChatGPT in order to improve the readability and language of the manuscript. After using this tool, the authors reviewed and edited the content as needed and take full responsibility for the content of the published article.

CRediT authorship contribution statement

Salma Bijou: Writing – review & editing, Writing – original draft, Visualization, Validation, Software, Methodology, Investigation, Formal analysis, Data curation, Conceptualization. **Lucie Kupková:** Writing – review & editing, Writing – original draft, Supervision, Resources, Project administration, Methodology, Investigation, Funding acquisition, Formal analysis, Data curation, Conceptualization. **Lucie Červená:** Writing – review & editing, Software, Methodology, Investigation, Data curation. **Jakub Lysák:** Investigation, Data curation.

Declaration of competing interest

The authors declare that they have no known competing financial interests or personal relationships that could have appeared to influence the work reported in this paper.

Acknowledgements

We would like to thank the Technology Agency of the Czech Republic for supporting this publication through the Programme Environment for Life, project SS05010124 “Assessment of the impact of land cover changes on local hydrology and climate in the Krkonoše Mts. National Park using remote sensing and hydrological modelling”, and project SS07010417 “Earth observation technologies for the surveillance activities of the Czech Environmental Inspectorate”; as well as the European Commission, CINEA Horizon Europe project no. 101081307 “Towards Sustainable Land-Use in the Context of Climate Change and Biodiversity in Europe (Europe-LAND)”. We also thank our colleagues from the Krkonoše National Park Administration and the local foresters, specifically Ing. Václav Jansa and Roman Rejzek, for their assistance with field data collection. Special thanks go to Dr. Jan Lubojacký for his help in defining the green stage substages.

Appendix A. Supplementary data

Supplementary data to this article can be found online at https://doi.org/10.1016/j.ecolind.2025.113869.

Data availability

Data will be made available on request.

References

Abdullah, H., Darvishzadeh, R., Skidmore, A.K., Groen, T.A., Heurich, M., 2018. European spruce bark beetle (Ips typographus, L.) green attack affects foliar reflectance and biochemical properties. Int. J. Appl. Earth Obs. Geoinf. 64, 199–209. https://doi.org/10.1016/j.jag.2017.09.009.

Abdullah, H., Darvishzadeh, R., Skidmore, A.K., Heurich, M., 2019. Sensitivity of Lsat-8 OLI and TIRS data to foliar properties of early-stage bark beetle (Ips typographus, L.) infestation. Remote Sens. 2019, 11, 398. Doi: 10.3390/rs11040398.

Adão, T., Hruška, J., Pádua, L., Bessa, J., Peres, E., Morais, R., Sousa, J.J., 2017. Hyperspectral imaging: a review on UAV-based sensors, data processing and applications for agriculture and forestry. Remote Sens. 9 (11), 1110. https://doi.org/10.3390/rs9111110.

Allen, C.D., Macalady, A.K., Chenchouni, H., Bachelet, D., McDowell, N., Vennetier, M., Kitzberger, T., Rigling, A., Breshears, D.D., Hogg, E.H., Gonzalez, P., Fensham, R., Zhang, Z., Castro, J., Demidova, N., Lim, J.H., Allard, G., Running, S.W., Semerci, A., Cobb, N., 2010. A global overview of drought and heat-induced tree mortality reveals emerging climate change risks for forests. Forest Ecol. Manag. 259 (4), 660–684. https://doi.org/10.1016/j.foreco.2009.09.001.

Anderegg, W.R.L., Trugman, A.T., Badgley, G., Anderson, C.M., Bartuska, A., Ciais, P., Cullenward, D., Field, C.B., Freeman, J., Goetz, S.J., Hicke, J.A., Huntzinger, D., Jackson, R.B., Nickerson, J., Pacala, S., Randerson, J.T., 2020. Climate-driven risks to the climate mitigation potential of forests. Science 368 (6497). https://doi.org/10.1126/science.aaz7005.

Angel, Y., Turner, D., Parkes, S., Malbeteau, Y., Lucieer, A., McCabe, M.F., 2020. Automated georectification and mosaicking of UAV-based hyperspectral imagery from push-broom sensors. Remote Sens. 12 (1), 1–25. https://doi.org/10.3390/RS12010034.

Baier, P., Pennerstorfer, J., Schopf, A., 2007. PHENIPS—a comprehensive phenology model of *Ips typographus* (L.) (Col., Scolytinae) as a tool for hazard rating of bark beetle infestation. For. Ecol. Manage. 249, 171–186. https://doi.org/10.1016/j.foreco.2007.05.023.

Barbedo, J.G.A., 2019. A review on the use of unmanned aerial vehicles and imaging sensors for monitoring and assessing plant stresses. Drones 3 (2), 1–27. https://doi.org/10.3390/drones3020040.

Bárta, V., Hanuš, J., Dobrovolný, L., Homolová, L., 2022. Comparison of field survey and remote sensing techniques for detection of bark beetle-infested trees. Forest Ecol. Manag. 506, 119984. https://doi.org/10.1016/j.foreco.2021.119984.

Bárta, V., Lukeš, P., Homolová, L., 2021. Early detection of bark beetle infestation in Norway spruce forests of Central Europe using Sentinel-2. Int. J. Appl. Earth Obs. Geoinf. 100, 102335. https://doi.org/10.1016/j.jag.2021.102335.

Berec, L., Doležal, P., Hais, M., 2013. Population dynamics of Ips typographus in the Bohemian Forest (Czech Republic): Validation of the phenology model PHENIPS and impacts of climate change. For. Ecol. Manag. 292, 1–9. https://doi.org/10.1016/j.foreco.2012.12.018.

Bijou, S., Kupková, L., Potůčková, M., Červená, L., Lysák, J., 2023. Evaluation of the bark beetle green attack detectability in spruce forest from multitemporal multispectral UAV imagery. ISPRS Ann. Photogramm. Remote Sens. Spatial Inf. Sci. X-1/W1-2023, 1033–1040. Doi: 10.5194/isprs-annals-X-1-W1-2023-1033-2023.

Borges, J.S., Marçal, A.R., Bioucas Dias, J.M., 2007. Evaluation of feature extraction and reduction methods for hyperspectral images. Proceedings of 26th EARSeL Symposium, New Developments and Challenges in Remote Sensing, 29, 265–274.

Botterweg, P.F., 1982. Dispersal and flight behaviour of the spruce bark beetle *Ips typographus* in relation to sex, size and fat content. Z. Angew. Entomol. 94, 466–489. https://doi.org/10.1111/j.1439-0418.1982.tb02594.x.

Bozzini, A., Brugnaro, S., Morgante, G., Santoiemma, G., Deganutti, L., Finozzi, V., Battisti, A., Faccoli, M., 2024. Drone-based early detection of bark beetle infested spruce trees differs in endemic and epidemic populations. Front. for. Glob. Change 7, 1385687. https://doi.org/10.3389/ffgc.2024.1385687.

Brázdil, R., Zahradník, P., Szabó, P., Chromá, K., Dobrovolný, P., Dolák, L., Trnka, M., Šeho, J., Suchánková, S., 2022. Meteorological and climatological triggers of notable past and present bark beetle outbreaks in the Czech Republic. Clim. Past 18 (9), 2155–2180. https://doi.org/10.5194/cp-18-2155-2022.

Callaway, B., Sant'Anna, P.H.C., 2021. Difference-in-differences with multiple time periods. J. Econom. 225 (2), 200–230. https://doi.org/10.1016/j.jeconom.2020.12.001.

Campbell, P.K.E., Rock, B.N., Martin, M.E., Neefus, C.D., Irons, J.R., Middleton, E.M., Albrechtova, J., 2004. Detection of initial damage in Norway spruce canopies using hyperspectral airborne data. Int. J. Remote Sens. 25 (24), 5557–5584. https://doi.org/10.1080/01431160410001726058.

Červená, L., Lysák, J., Potůčková, M., Kupková, L., 2020. Zkušenosti se zpracováním hyperspektrálních dat pořízených UAV. Presented at GIS Ostrava 2020 – Prostorová data pro Smart City a Smart Region. Doi: 10.31490/9788024843988-4.

ČHMÚ, 2025. Czech Hydrometeorological Institute. Available from: https://www.chmi.cz/historicka-data/pocasi/denni-data/Denni-data-dle-z.-123-1998-Sb.

Clark, M.L., Roberts, D.A., Clark, D.B., 2005. Hyperspectral discrimination of tropical rain forest tree species at leaf to crown scales. Remote Sens. Environ. 96 (3–4), 375–398. https://doi.org/10.1016/j.rse.2005.03.009.

Dalponte, M., Cetto, R., Marinelli, D., Andreatta, D., Salvadori, C., Pirotti, F., Frizzera, L., Gianelle, D., 2023. Spectral separability of bark beetle infestation stages: a single-tree time-series analysis using Planet imagery. Ecol. Indic. 153, 110349. https://doi.org/10.1016/j.ecolind.2023.110349.

Dalponte, M., Ørka, H.O., Ene, L.T., Gobakken, T., Næsset, E., 2014. Tree crown delineation and tree species classification in boreal forests using hyperspectral and ALS data. Remote Sens. Environ. 140, 306–317. https://doi.org/10.1016/j.rse.2013.09.006.

Dao, P.B., 2022. On Wilcoxon rank sum test for condition monitoring and fault detection of wind turbines. Appl. Energy 318, 119209. https://doi.org/10.1016/j.apenergy.2022.119209.

Doležal, P., Sehnal, F., 2007. Effects of photoperiod and temperature on the development and diapause of the bark beetle Ips typographus. J. Appl. Entomol. 131 (3), 165–173. https://doi.org/10.1111/j.1439-0418.2006.01123.x.

Einzmann, K., Atzberger, C., Pinnel, N., Glas, C., Böck, S., Seitz, R., Immitzer, M., 2021. Early detection of spruce vitality loss with hyperspectral data: results of an experimental study in Bavaria, Germany. Remote Sens. Environ. 266, 112676. https://doi.org/10.1016/j.rse.2021.112676.

Forzieri, G., Girardello, M., Ceccherini, G., Spinoni, J., Feyen, L., Hartmann, H., Beck, P. S.A., Camps-Valls, G., Chirici, G., Mauri, A., Cescatti, A., 2021. Emergent vulnerability to climate-driven disturbances in European forests. Nat. Commun. 12 (1). https://doi.org/10.1038/s41467-021-21399-7.

Fu, L., Zhou, L., Wu, P., Zhu, Z., Yu, Z., Wang, D., 2022. Evaluating the causal effects of emissions trading policy on emission reductions based on nonlinear difference-in-difference model. Sustainability (Switzerland) 14 (23). https://doi.org/10.3390/su142315726.

Hase, N., Doktor, D., Rebmann, C., Dechant, B., Mollenhauer, H., Cuntz, M., 2022. Identifying the main drivers of the seasonal decline of near-infrared reflectance of a temperate deciduous forest. Agric. For. Meteorol. 313, 108746. https://doi.org/10.1016/j.agrformet.2021.108746.

Hellwig, F.M., Stelmaszczuk-Górska, M.A., Dubois, C., Wolsza, M., Truckenbrodt, S.C., Sagichewski, H., Chmara, S., Bannehr, L., Lausch, A., Schmullius, C., 2021. Mapping European spruce bark beetle infestation at its early phase using gyrocopter-mounted hyperspectral data and field measurements. Remote Sens. 13 (22). https://doi.org/10.3390/rs13224659.

Hlásny, T., König, L., Krokene, P., Lindner, M., Montagné-Huck, C., Müller, J., Qin, H., Raffa, K.F., Schelhaas, M.J., Svoboda, M., Viiri, H., Seidl, R., 2021. Bark beetle outbreaks in Europe: State of knowledge and ways forward for management. Curr. For. Rep. 7 (3), 138–165. https://doi.org/10.1007/s40725-021-00142-x.

Housecroft, C.E., 2023. The growing problem of the spruce bark beetle. Chimia 77 (9), 623–624. https://doi.org/10.2533/chimia.2023.623.

Huo, L., Koivumäki, N., Oliveira, R.A., Hakala, T., Markelin, L., Näsi, R., Suomalainen, J., Polvivaara, A., Junttila, S., Honkavaara, E., 2024. Bark beetle pre-emergence detection using multi-temporal hyperspectral drone images: Green shoulder indices can indicate subtle tree vitality decline. ISPRS J. Photogramm. Remote Sens. 216, 200–216. https://doi.org/10.1016/j.isprsjprs.2024.07.027.

Huo, L., Lindberg, E., Bohlin, J., Persson, H.J., 2023a. Assessing the detectability of European spruce bark beetle green attack in multispectral drone images with high spatial and temporal resolutions. Remote Sens. Environ. 287, 113484. https://doi.org/10.1016/j.rse.2023.113484.

Huo, L., Persson, H.J., Bohlin, J., Lindberg, E., 2023b. Green attack or overfitting? Comparing machine-learning- and vegetation-index-based methods to early detect European spruce bark beetle attacks using multispectral drone images. In: IGARSS 2023–2023 IEEE International Geoscience and Remote Sensing Symposium. https://doi.org/10.1109/IGARSS52108.2023.10282624.

Huo, L., Persson, H.J., Lindberg, E., 2021. Early detection of forest stress from European spruce bark beetle attack, and a new vegetation index: Normalized distance red & SWIR (NDRS). Remote Sens. Environ. 255, 112240. https://doi.org/10.1016/j.rse.2020.112240.

Jacoby, O., Lischke, H., Wermelinger, B., 2019. Climate change alters elevational phenology patterns of the European spruce bark beetle (Ips typographus). Glob. Chang. Biol. 25, 4048–4063. https://doi.org/10.1111/gcb.14766.

Jones, K.L., Shegelski, V.A., Marculis, N.G., Wijerathna, A.N., Evenden, M.L., 2019. Factors influencing dispersal by flight in bark beetles (Coleoptera: Curculionidae: Scolytinae): from genes to landscapes. Can. J. For. Res. 49 (9), 1024–1041. https://doi.org/10.1139/cjfr-2018-0304.

Jönsson, A.M., Harding, S., Bärring, L., Ravn, H.P., 2007. Impact of climate change on the population dynamics of *Ips typographus* in southern Sweden. Agric. For. Meteorol. 146 (1–2), 70–81. https://doi.org/10.1016/j.agrformet.2007.05.006.

Junttila, S., Näsi, R., Koivumäki, N., Imangholiloo, M., Saarinen, N., Raisio, J., Holopainen, M., Hyyppä, H., Hyyppä, J., Lyytikäinen-Saarenmaa, P., Vastaranta, M., Honkavaara, E., 2022. Multispectral imagery provides benefits for mapping spruce tree decline due to bark beetle infestation when acquired late in the season. Remote Sens. 14 (4). https://doi.org/10.3390/rs14040909.

Kautz, M., Schopf, R., Ohser, J., 2013. The "sun-effect": microclimatic alterations predispose forest edges to bark beetle infestations. Eur. J. For. Res. 132, 453–465. https://doi.org/10.1007/s10342-013-0685-2.

Kautz, M., Feurer, J., Adler, P., 2024. Early detection of bark beetle (Ips typographus) infestations by remote sensing – a critical review of recent research. For. Ecol. Manag. 556, 121595. https://doi.org/10.1016/j.foreco.2023.121595.

Kautz, M., Peter, F.J., Harms, L., Kammen, S., Delb, H., 2023. Patterns, drivers and detectability of infestation symptoms following attacks by the European spruce bark beetle. J. Pest Sci. 96, 403–414. https://doi.org/10.1007/s10340-022-01490-8.

Klouček, T., Komárek, J., Kycko, M., Hrach, K., Modlinger, R., 2024. Detection of bark beetle infestation using UAV-borne multi-spectral imagery: a case study of the mountain Norway spruce managed forest in the Czech Republic. Remote Sens. (Under Review) 1–13. https://doi.org/10.3389/ffgc.2024.1215734.

Klouček, T., Komárek, J., Surový, P., Hrach, K., Janata, P., Vašíček, B., 2019. The use of UAV mounted sensors for precise detection of bark beetle infestation. Remote Sens. 11 (13). https://doi.org/10.3390/rs11131561.

Knutzen, F., Averbeck, P., Barrasso, C., Bouwer, L.M., Gardiner, B., Grünzweig, J.M., Hänel, S., Haustein, K., Johannessen, M.R., Kollett, S., Pietikäinen, J.P., Pietras-Couffignal, K., Pinto, J.G., Rechid, D., Rousi, E., Russo, A., Suarez-Gutierrez, L., Wendler, J., Xoplaki, E., Gliksman, D., 2023. Impacts and damages of the European multi-year drought and heat event 2018–2022 on forests, a review. Egusphere Preprint 1–56.

Kupková, L., Potůčková, M., Lhotáková, Z., Albrechtová, J., 2018. Forest cover and disturbance changes, and their driving forces: a case study in the Ore Mountains, Czechia, heavily affected by anthropogenic acidic pollution in the second half of the 20th century. Environ. Res. Lett. 13 (9). https://doi.org/10.1088/1748-9326/aadd2c.

Lausch, A., Heurich, M., Gordalla, D., Dobner, H.J., Gwillym-Margianto, S., Salbach, C., 2013. Forecasting potential bark beetle outbreaks based on spruce forest vitality using hyperspectral remote-sensing techniques at different scales. For. Ecol. Manag. 308, 76–89. https://doi.org/10.1016/j.foreco.2013.07.043.

Lindner, M., Maroschek, M., Netherer, S., Kremer, A., Barbati, A., Garcia-Gonzalo, J., Seidl, R., Delzon, S., Corona, P., Kolström, M., Lexer, M.J., Marchetti, M., 2010. Climate change impacts, adaptive capacity, and vulnerability of European forest ecosystems. For. Ecol. Manag. 259 (4), 698–709. https://doi.org/10.1016/j.foreco.2009.09.023.

Lubojacký, J., Knížek, M., Liška, J., 2018. Lýkožrout smrkový Ips typographus (L.) – *Spruce Bark Beetle* Ips typographus *(L.)*. Lesn. Práce 5 (2018), 1–4. http://www.silvarium.cz/images/letaky-los/2018/2018_kurovci_symptomy_napadeni_kurovcoveho_drivi_ve_smrkovych_porostech.pdf.

Lubojacký, J., Lorenc, F., Véle, A., Knížek, M., 2023. Výskyt lesních škodlivých faktorů v Česku v roce 2022 – Occurrence of forest harmful agents in the Czech Republic in 2022. Zprav. Lesn. Ochr.

Maes, J., Bruzón, A.G., Barredo, J.I., Vallecillo, S., Vogt, P., Marí Rivero, I., Santos-Martín, F., 2023. Accounting for forest condition in Europe based on an international statistical standard. Nat. Commun. 14 (1), 1–15. https://doi.org/10.1038/s41467-023-39434-0.

Magstadt, S., Gwenzi, D., Madurapperuma, B., 2021. Can a remote sensing approach with hyperspectral data provide early detection and mapping of spatial patterns of black bear bark stripping in coast redwoods? Forests 12 (3). https://doi.org/10.3390/f1203.

Marx, A., Clasen, A., May, J., König, S., Kleinschmit, B., Förster, M., 2024. Imaging spectroscopy for bark beetle detection in Norway spruce and the relevance of the red-edge spectral range. Int. J. Appl. Earth Obs. Geoinf. 133, 104100. https://doi.org/10.1016/j.jag.2024.104100.

Mcilwaine, B., Rivas Casado, M., Leinster, P., 2019. Using 1st derivative reflectance signatures within a remote sensing framework to identify macroalgae in marine environments. Remote Sens. 11 (6), 1–23. https://doi.org/10.3390/rs11060704.

Minařík, R., Langhammer, J., 2016. Use of a multispectral UAV photogrammetry for detection and tracking of forest disturbance dynamics. ISPRS Arch. 41, 711–718. https://doi.org/10.5194/isprsarchives-XLI-B8-711-2016.

Müller, M., Olsson, P.O., Eklundh, L., Jamali, S., Ardö, J., 2022. Features predisposing forest to bark beetle outbreaks and their dynamics during drought. For. Ecol. Manag. 523, 120480. https://doi.org/10.1016/j.foreco.2022.120480.

Murray, J., 2006. Forestry in the Czech and Slovak Republics. Q. J. for. 100, 123–128.

Nardi, D., Bozzini, A., Morgante, G., Gaccione, A., Finozzi, V., Battisti, A., 2023. Participatory ground data are complementary to satellite bark beetle detection. Ann. For. Sci. 80 (1). https://doi.org/10.1186/s13595-023-01216-5.

Näsi, R., Honkavaara, E., Lyytikäinen-Saarenmaa, P., Blomqvist, M., Litkey, P., Hakala, T., Viljanen, N., Kantola, T., Tanhuanpää, T., Holopainen, M., 2015. Using UAV-based photogrammetry and hyperspectral imaging for mapping bark beetle damage at tree-level. Remote Sens. (Basel) 7 (11), 15467–15493. https://doi.org/10.3390/rs71115467.

Niemann, K.O., Visintini, F., 2005. Assessment of potential for remote sensing detection of bark beetle-infested areas during green attack: a literature review. Natural Resources Canada, Canadian Forest Service, Pacific Forestry Centre, Victoria, BC. Mountain Pine Beetle Initiative Working Paper 2005-02. 14 p.

Padma, S., Sanjeevi, S., 2014. Jeffries Matusita based mixed-measure for improved spectralmatching in hyperspectral image analysis. Int. J. Appl. Earth Obs. Geoinf. 32 (1), 138–151. https://doi.org/10.1016/j.jag.2014.04.001.

Pan, J., Ye, X., Shao, F., Liu, G., Liu, J., Wang, Y., 2024. Impacts of pine species, infection response, and data type on the detection of *Bursaphelenchus xylophilus* using close-range hyperspectral remote sensing. Remote Sens. Environ. 315, 114468. https://doi.org/10.1016/j.rse.2024.114468.

Pirtskhalava-Karpova, N., Trubin, A., Karpov, A., Jakuš, R., 2024. Drought Initialised Bark Beetle Outbreak in Central Europe: Meteorological Factors and Infestation Dynamic. Forest Ecology and Management, 554(September 2023). Doi: 10.1016/j.foreco.2023.121666.

Prăvălie, R., 2018. Major perturbations in the Earth's forest ecosystems. Possible implications for global warming. Earth Sci. Rev. 185 (May), 544–571. https://doi.org/10.1016/j.earscirev.2018.06.010.

Pretzsch, H., del Río, M., Arcangeli, C., Bielak, K., Dudzinska, M., Forrester, D.I., Klädtke, J., Kohnle, U., Ledermann, T., Matthews, R., Nagel, J., Nagel, R., Ningre, F., Nord-Larsen, T., Biber, P., 2023. Forest growth in Europe shows diverging large regional trends. Sci. Rep. 13 (1), 1–12. https://doi.org/10.1038/s41598-023-41077-6.

Sen, R., Goswami, S., Chakraborty, B., 2019. Jeffries-Matusita distance as a tool for feature selection. In: 2019 International Conference on Data Science and Engineering (ICDSE), pp. 15–20. https://doi.org/10.1109/ICDSE47409.2019.8971800.

Sikorski, P., Archiciński, P., Ciężkowski, W., Kościelny, M., Kościelna, A., Schwerk, A., 2023. Forest ecosystem disturbance affects tree Dieback from Ips engraver beetles, evidence from UAV multispectral mapping. Sylwan 167 (1), 13–25. https://doi.org/10.26202/sylwan.2022078.

StataCorp., 2023. Stata Statistical Software: Release 18. StataCorp LLC, College Station, TX.

Stříbrská, B., Hradecký, J., Čepl, J., Modlinger, R., Tomášková, I., Jirošová, A., 2023. Physiological and biochemical indicators in Norway spruces freshly infested by Ips typographus: potential for early detection methods. Front. For. Global Change 6, 1–13. https://doi.org/10.3389/ffgc.2023.1197229.

Trubin, A., Kozhoridze, G., Zabihi, K., Modlinger, R., Singh, V.V., Surový, P., Jakuš, R., 2024. Detection of green attack and bark beetle susceptibility in Norway spruce: Utilizing PlanetScope multispectral imagery for tri-stage spectral separability analysis. For. Ecol. Manage. 560. https://doi.org/10.1016/j.foreco.2024.121838.

Umebayashi, T., Fukuda, K., Haishi, T., Sotooka, R., Zuhair, S., Otsuki, K., 2011. The developmental process of xylem embolisms in pine wilt disease monitored by multipoint imaging using compact magnetic resonance imaging. Plant Physiol. 157 (1), 579–589. https://doi.org/10.1104/pp.110.170282.

Urbanek Krajnc, A., 2009. A temporal analysis of antioxidative defense responses in the phloem of *Picea abies* after attack by *Ips typographus*. Tree Physiol. 29 (8), 1059–1068. https://doi.org/10.1093/treephys/tpp041.

Wang, S., Rao, Y., Chen, J., Liu, L., Wang, W., 2021. Adopting 'difference-in-differences' method to monitor crop response to agrometeorological hazards with satellite data: a case study of dry-hot wind. Remote Sens. (Basel) 13 (3), 1–22. https://doi.org/10.3390/rs13030482.

Webb, C.R., Blake, M., Gilligan, C.A., 2024. Phenology of the spruce bark beetle Ips typographus in the UK under past, current and future climate conditions. Plants People Planet. https://doi.org/10.1002/ppp3.10583.

Wermelinger, B., Seifert, M., 1998. Analysis of the temperature dependent development of the spruce bark beetle Ips typographus (L.) (Col., Scolytidae). J. Appl. Entomol. 122 (4), 185–191. https://doi.org/10.1111/j.1439-0418.1998.tb01482.x.

Wilcoxon, F., 1945. Individual comparisons by ranking methods. Biometrics 1 (6), 80–83. https://doi.org/10.2307/3001968.

Xie, H., Tan, X., Yang, C., Li, C., 2022. Does urban forest control smog pollution? Evidence from National Forest City Project in China. Sustainability (Switzerland) 14 (19). https://doi.org/10.3390/su141912897.

Zhang, H., Jiao, X., Zha, T., Lv, X., Ni, Y., Zhang, Q., Wang, J., Ma, L., 2023a. Developmental dynamics and driving factors of understory vegetation: a case study of three typical plantations in the Loess Plateau of China. Forests 14 (12). https://doi.org/10.3390/f14122353.

Zhang, L., Jin, J., Wang, L., Rehman, T.U., Gee, M.T., 2023b. Elimination of leaf angle impacts on plant reflectance spectra using fusion of hyperspectral images and 3D point clouds. Sensors 23 (1). https://doi.org/10.3390/s23010044.

Zimová, S., Dobor, L., Hlásny, T., Rammer, W., Seidl, R., 2020. Reducing rotation age to address increasing disturbances in central Europe: potential and limitations. For. Ecol. Manage. 475, 118408. https://doi.org/10.1016/j.foreco.2020.118408.